Kinetic studies of solid foam catalysts for the production of sugar alcohols: Xylitol from biomass resources

Araujo Barahona, German; Goicoechea-Torres, Alberto; Eränen, Kari; Latonen, Rose-Marie; Tirri, Teija; Smeds, Annika I.; Murzin, Dmitry; García-Serna, Juan; Salmi, Tapio

Published in:
Chemical Engineering Science

DOI:
10.1016/j.ces.2023.119130

Published: 05/11/2023

Document Version
Final published version

Document License
CC BY

Chemical Engineering Science 281 (2023) 119130

Contents lists available at ScienceDirect

Chemical Engineering Science

journal homepage: www.elsevier.com/locate/ces

Kinetic studies of solid foam catalysts for the production of sugar alcohols: Xylitol from biomass resources

German Araujo-Barahona [a,b], Alberto Goicoechea-Torres [a,b], Kari Eränen [a], Rose-Marie Latonen [c], Teija Tirri [d], Annika Smeds [d], Dmitry Murzin [a], Juan García-Serna [b], Tapio Salmi [a,*]

[a] Laboratory of Industrial Chemistry and Reaction Engineering (TKR), Johan Gadolin Process Chemistry Centre (PCC), Åbo Akademi University, FI-20500 Turku, Åbo Finland

[b] Grupo de Tecnologías a Presión (PressTech), Instituto de Bioeconomía de la Universidad de Valladolid (BioEcoUVa), Departamento de Ingeniería Química y Tecnología del Medio Ambiente, Escuela de Ingenierías Industriales, Universidad de Valladolid, 47011 Valladolid, Spain

[c] Laboratory of Molecular Science and Engineering, Johan Gadolin Process Chemistry Centre, Åbo Akademi University, FI-20500 Turku, Åbo Finland

[d] Laboratory of Natural Materials Technology, Johan Gadolin Process Chemistry Centre, Åbo Akademi University, FI-20500 Turku, Åbo Finland

ARTICLE INFO

Keywords:
Hydrogenation
Sugar alcohols
Sweeteners
Structured catalyst
Rotating foam reactor
Pore former

ABSTRACT

Structured catalysts, such as solid foams, represent a very promising technology for continuous and stable production of high-value compounds derived from biomass, traditionally produced with batch and semibatch technologies using suspended catalysts. However, the synthesis of structured catalysts presents additional challenges related to their structure and the generation of porous coatings with suitable properties for dispersing the catalytically active phase on the support.

This work was focused on synthesizing a Ru/C solid foam catalyst and investigating its activity in the selective hydrogenation of xylose to xylitol under different operational conditions. The carbon coating, the key step of preparation, was based on the formation and pyrolysis of poly(furfuryl alcohol) in the presence of different amounts of poly(ethylene glycol) (PEG; M = 8 kDa) as a pore former, which enabled tuning the support porosity. Thus, the catalyst prepared with 5 wt% PEG presented a micro-to-mesopores volume ratio of 1, and a good dispersion of Ru nanoparticles, as well as a better stability compared to the catalyst prepared without PEG.

The extensive kinetic data collected in this work were mathematically modelled using three different approaches to elucidate the reactant adsorption mode: a non-competitive adsorption model, a non-competitive adsorption model considering the effect of temperature, and a semi-competitive adsorption model. The non-competitive temperature-dependent model displayed better performance in terms of fitting and reliability of the estimated parameters and predicted the adsorption of xylose as an endothermic process. On the other hand, the semi-competitive model gave similar results in terms of fitting and a value for the competitiveness factor of 0.74, which matches the hypothesis that the larger molecules, sugars, can occupy most of the active sites, while some interstitial sites remain accessible for hydrogen adsorption. The modelling results revealed a complex mode of sugar adsorption on the catalyst surface. This modelling concept can be applied to any system in which the molecule sizes are very different.

1. Introduction

Sustainability lies in the idea of a welfare society with the urgency that what was enunciated as “future generations” becomes clearer and clearer every day that it is the present. The 17 Sustainable Development Goals (SDGs) established in 2015 by the United Nations General Assembly aim to achieve a better future for the world within the framework of the 2030 Agenda (UN, 2017). The population has continued to grow in recent decades, and human activities have not always been sufficiently refined, resulting in increased pollution, climate change, global warming, and the depletion of natural resources. From a chemical engineering perspective, we can improve many activities, industrial practices, and products towards sustainability. In this context, the use of lignocellulosic biomass as feedstock for the chemical industry is a promising approach and a challenge that has motivated

* Corresponding author.
E-mail address: tapio.salmi@abo.fi (T. Salmi).

https://doi.org/10.1016/j.ces.2023.119130
Received 17 February 2023; Received in revised form 24 July 2023; Accepted 25 July 2023
Available online 29 July 2023

Notation

Description

$C_{*'}$	Concentration of the active sites *'[mol•mol^{-1}]
$C_{*'H}$	Hydrogen concentration on active sites *'[mol•mol^{-1}]
C_{*X}	Xylose concentration on active sites *[mol•mol^{-1}]
$C_{Calc.i}$	Predicted concentration from the model.[mol•L^{-1}]
$C_{Exp,i}$	Experimental concentration.[mol•L^{-1}]
C_{H_2}	Concentration of hydrogen in the liquid phase.[mol•L^{-1}]
C_*	Concentration of the active sites *[mol•mol^{-1}]
C_0	Total concentration of active sites */ Total concentration of primary sites in the semi-competitive model.[mol•mol^{-1}]
C'_0	Total concentration of active sites *'.[mol•mol^{-1}]
C_X	Xylose concentration in the liquid phase.[mol•L^{-1}]
C_{XOH}	Xylitol concentration in the liquid phase.[mol•L^{-1}]
E_A	Activation energy.[kJ•mol^{-1}]
K_{H_2}	Merged parameter for hydrogen.[bar^{-1}]
I_D	Integrated intensities of the D band.[a.u.]
I_G	Integrated intensities of the G band.[a.u.]
K_{LH_2}	Henry's law solubility constant for hydrogen.[mol•bar^{-1}•L^{-1}]
k_X	Kinetic constant for xylose hydrogenation[mol•g$_{Ru}^{-1}$•min^{-1}]
K_X	Adsorption parameter for xylose.[L•mol^{-1}]
$K_{X,\,90^\circ C}$	Adsorption parameter for xylose at 90 °C.[L•mol^{-1}]
K_H	Adsorption parameter for hydrogen.[bar^{-1}]
M	Molar mass.[kDa]
m	Number of active sites required for the adsorption of xylose.
m_{cat}	Mass of catalyst.[g]
P_{H_2}	Hydrogen pressure.[bar]
Q	Objective function, residual sum of squares (RSS).[L^2•mol^{-2}]
R	Gas constant.[J·K^{-1}·mol^{-1}]
r_X	Reaction rate of xylose consumption.[mol•gRu^{-1}•min^{-1}]
R^2	Coefficient of determination.[%]
T	Temperature.[K]
$\bar{T}$	Reference temperature.[K]
V_L	Volume of liquid[L]
α	Competitiveness factor
ΔH_{H_2}	Adsorption enthalpy for hydrogen.[kJ•mol^{-1}]
ΔH_X	Adsorption enthalpy for xylose.[kJ•mol^{-1}]
κ_X	Merged parameter of xylose[L•gRu^{-1}•min^{-1}•bar^{-1}]
$\kappa_{X\,90^\circ C}$	Merged parameter for xylose at 90 °C.[L•gRu^{-1}•min^{-1}•bar^{-1}]
ρ_B	Bulk density[gRu•L^{-1}]

Abbreviations

A.O.	Anodic Oxidation
A.U.	Arbitrary units
BSTFA	N,O-Bis(trimethylsilyl)trifluoroacetamide
TCD	Thermal conductivity detector
TMCS	Trimethylsilyl chloride

extensive research and development efforts in recent years (Aguilar et al., 2018; Ajao et al., 2018; Ruppert et al., 2012; Xu et al., 2019). In this sense, a prime example of the application of the so-called second generation biorefinery concept is the production of sugar alcohols (e.g., sorbitol, xylitol, arabitol, galactitol), molecules with diverse applications in alimentary, pharmaceutical, and cosmetic industries (Delgado Arcaño et al., 2020; Murzin et al., 2016; Redina et al., 2022).

Among the most industrially relevant sugar alcohols, xylitol stands out for its high sweetening strength and a low caloric content. It is used as a substitute for sucrose in bakery and confectionery products, especially chewing gum (Research and Markets, 2021a). Moreover, many xylitol-based oral health products have been commercialized because this sugar alcohol reduces the incidence of dental caries by 85% (Mäkinen et al., 1998), promotes saliva production (Autio, 2002), and inhibits plaque growth (Kandelman, 1997). Other health-promoting applications of xylitol include its potential use as a treatment for acute otitis media (Erramouspe and Heyneman, 2000), osteoporosis due to its enhancing effect on calcium absorption (Mattila et al., 1996), respiratory diseases (Zabner et al., 2000), and colon diseases, owing to its ability to improve the development of the microbiota (Mitchell, 2007).

Xylitol, with a global market size of nearly 900 million euros in 2021 and a projected size of ca. 1200 million euros by 2027 with an annual growth rate of 5.1 % (Research and Markets, 2021b), has been classified in the list of high-value compounds from biomass by the US National Renewable Energy Laboratory (NREL) (Redina et al., 2022; Werpy and Petersen, 2004) and in the final report of 2015 of the European Commission for the Directorate General of Energy (Delgado Arcaño et al., 2020; Taylor et al., 2015). An apparent reason for this is its potential use as a building block to produce other relevant chemicals such as ethylene glycol, propylene glycol, lactic acid, glycerol, xylonic acid, polyesters, and nylons (Delgado Arcaño et al., 2020).

Conventional production of xylitol is carried out through catalytic hydrogenation of xylose, which is obtained from hemicelluloses such as xylans by acid hydrolysis in the presence of homogeneous or heterogeneous catalysts. Purified xylose is hydrogenated at hydrogen pressures of 5–60 bar and temperatures of 80–140 °C in the presence of a finely dispersed Ni-based catalyst, conventionally known as Raney nickel or sponge nickel (Murzin et al., 2016). Although this is a relatively well-established industrial process, Raney nickel suffers from serious drawbacks such as pyrophoricity, formation of poisonous by-products, deactivation, leaching, and, in the conventional finely dispersed form, its use is limited to batch operation. Therefore, ruthenium-based catalysts, have been proposed to replace nickel (Hoffer et al., 2003) because of the high catalytic activity of ruthenium for this reaction, as demonstrated by experiments on ruthenium on activated carbon (Sifontes Herrera et al., 2011) and ruthenium on polymeric supports (Sapunov et al., 2013), as well as by theoretical considerations (Akpe et al., 2021).

On the other hand, structured catalysts offer advantageous characteristics for continuous and stable production in the fine chemical industry, which is mainly governed by batch processes. This type of catalysts, e.g., solid foams, monoliths, and 3D printed structures, combines the benefits of slurry and shaped-body catalyst technologies, i.e., thin catalyst layers ensure high effectiveness factors, and their open structures allows operation with low pressure drops (Italiano et al., 2018; Tronconi et al., 2014). Furthermore, metallic foams provide excellent mechanical properties and a disruptive flow path that improves the gas–liquid dispersion and heat transfer in three-phase systems (Ho et al., 2019).

The preparation of foam structures for catalytic applications requires a wash-coating step that allows the incorporation of a porous support layer to enable the dispersion of catalytically active metals (Wenmakers et al., 2010). For sugar hydrogenation, carbon is a suitable support with adequate porosity and interaction with ruthenium nanoparticles (Hoffer et al., 2003).

Carbon coating techniques utilized for structured catalysts preparation usually include the formation and pyrolysis of a polymer precursor layer. A good example of this is poly(furfuryl alcohol) (P(FA)) (Araujo-Barahona et al., 2022; Lali et al., 2015b; Moreno-Castilla et al., 1980; Najarnezhadmashhadi et al., 2020; Schimpf et al., 2004), which has two advantages—a high carbon yield (above 40%), and its monomer,

furfuryl alcohol, typically originates from renewable agricultural sources such as wood wastes and food crop residues (Mariscal et al., 2016).

The carbons obtained from poly(furfuryl alcohol) pyrolysis are mainly microporous materials (Schlumberger and Thommes, 2021). Therefore, several activation processes have been utilized to create mesopores inside PFA-derived carbons, for example, physical activation with carbon dioxide, oxygen, and water vapor as well as chemical activation with reagents such as acids (Lorenc-Grabowska and Rutkowski, 2018; Sricharoenchaikul et al., 2008). Another alternative is the addition of pore-forming substances inside the carbon precursor polymer, combined with physical activation (Lafyatis et al., 1991; Strano et al., 2003).

From the point of view of preserving the mechanical stability of metallic structural supports, such as aluminium foams, the addition of non-carbonizing pore formers, such as polyethylene glycol (PEG), is considered a more feasible option since it allows lower activation temperatures and avoids exposure to corrosive chemicals. According to Strano et al. (2003), PEG acts as a volume exclusion agent during the growth and concatenation of carbon mesogens (liquid crystal phase) in the pyrolysis process, which results in tailoring of the obtained porosity of the carbon.

The objective of this work was to develop a Ru/C foam catalyst based on the formation and pyrolysis of poly(furfuryl alcohol) with improved mesoporosity by adding a high molecular mass poly(ethylene glycol) as a pore former and to study its catalytic activity and the reaction kinetics of xylose hydrogenation at different temperatures, hydrogen pressures, and initial concentrations. Mathematical models for the kinetic data were developed based on plausible surface reaction mechanisms, i.e., non-competitive adsorption of sugar molecules and hydrogen, as well as a semi-competitive adsorption model.

2. Experimental section

2.1. Catalyst synthesis

The preparation of the catalyst consisted of the following steps: anodic oxidation, carbon coating, acid treatment, ruthenium incorporation, and *ex-situ* reduction. The synthesis process is explained in detail in a previous article by our research group (Araujo-Barahona et al., 2022). A summary of this is provided in this section.

Cylindrical pieces (33 mm length and 11 mm diameter) cut from a commercially available aluminium open-cell foam sheet (Goodfellow Cambridge Ltd.) with 96% porosity were anodized for one hour under an electrical current of 2 A and then calcined for four hours at 600 °C. The electrolyte solution used consisted of 100 mL of 1.6 mol/L sulfuric acid (Sigma-Aldrich; 96 wt%) and 60 g/L of aluminium sulphate hexadecahydrate (Fluka; 98 wt%).

The carbon coating proceeded via poly(furfuryl alcohol) pyrolysis — three foam pieces were attached to a crossed blade stirrer shaft and immersed in a mixture consisting of 136.2 g of furfuryl alcohol (Sigma-Aldrich; 98 wt%), 0.84 g of oxalic acid dihydrate (Sigma-Aldrich; 99.5 wt%), and 16.7 g of distilled water. The foams were rotated at 200 rpm while the temperature was increased at a rate of 2 °C/min to 110 °C. The heating was then regulated manually to obtain a curing time for the polymer of ca. one hour in a temperature range of 110–130 °C. Different amounts of polyethylene glycol (M = 8 kDa; Sigma-Aldrich) (0–15 wt%) were added to the mixture in the final curing stage (approx. at 50th minute). The samples were labelled according to the percentage of PEG added as F0PEG, F3PEG, F5PEG, and F15PEG.

The excess polymer on the foams was removed by rotating them for five minutes at 1000 rpm using a centrifugation-like effect. Subsequent polymer pyrolysis was carried out at 550 °C in a furnace with a nitrogen flow of 2000 mL/min for five hours, followed by an activation step at 380 °C under an airflow of 1000 mL/min for two hours. The obtained carbon-coated foams were immersed in a 5 wt% nitric acid solution (Sigma-Aldrich; 70 wt%) for two hours, after which they were washed and oven-dried for two more hours at 70 °C.

The ruthenium incorporation was performed by incipient wetness impregnation of a 0.6 mol/L solution of Ru(III) nitrosyl nitrate (1.4% wt. Ru, diluted in nitric acid solution; Sigma-Aldrich). The precursor was dripped onto the carbon surface in steps of approximately 0.4 g of solution. The drying time per step was 24 h at 110 °C. Finally, the catalysts were reduced *ex-situ* at 300 °C for five hours under a 100 mL/min hydrogen flow. The reduction temperature was selected based on Temperature-Programmed Reduction (TPR) experiments on the catalyst.

2.2. Characterization techniques

The decomposition patterns of the carbon precursor polymers were obtained by heating 20 mg of sample from room temperature to 1000 °C following a ramp of 5 °C/min in a nitrogen atmosphere using a SDT 650 simultaneous thermal analyzer.

The morphology of the carbon coatings was studied using scanning electron microscopy (SEM; Zeiss Leo Gemini 1530). The size distribution of the ruthenium nanoparticles deposited on the foams was determined by transmission electron microscopy (TEM, JEM 1400 Plus Transmission Electron Microscope); 1000 particles per sample were measured in ImageJ software.

Raman spectroscopy was employed to characterize the carbon coating obtained by adding different PEG amounts in the polymer precursor. Raman spectra were recorded with a Renishaw Ramascope imaging microscope. An Ar-ion laser with an excitation wavelength of 514 nm and power of 25 mW was utilized to record the spectra in the wavenumber range of 400–2000 cm^{-1}. The spectrometer was calibrated against a silicon standard (520 cm^{-1}).

The ruthenium content of the catalysts and the degree of leaching during the kinetic experiments were determined using Inductively Coupled Plasma Optical Emission Spectroscopy (ICP-OES, PerkinElmer, Optima 5300 DV). The solid samples (0.1 g) were dissolved in a mixture of 3 mL of sulfuric acid (Sigma-Aldrich; 96 wt%) and 3 mL of nitric acid (Sigma-Aldrich; 65 wt%) while the liquid samples before and after each selected catalytic experiment were taken and analysed directly through ICP-OES (40 bar; 60 °C, 90 °C, 100 °C, and 120 °C).

Temperature-Programmed Reduction (Microtrac MRB Catalyst Analyzer Belcat II) measurements were performed to establish adequate *ex-situ* reduction conditions for the prepared catalysts. The TPR measurements were conducted in the temperature range of 30–700 °C following a ramp of 10 °C/min. A gas flow of 5 mol% hydrogen in argon (30 cm3/min) was used.

The Dubinin-Radushkevich and Brunauer–Emmett–Teller (BET) models were applied to calculate the specific surface areas, and the non-local density function theory (NLDFT) model was used to estimate the pore size distribution of the prepared catalysts assuming a slit pore geometry (Medek, 1977). Nitrogen physisorption isotherms (77 K) were obtained using a Micromeritics 3Flex-3500 sorptometer. The samples were outgassed for 24 h at 300 °C before the analysis.

2.3. Kinetic hydrogenation experiments

The Screening of the prepared catalysts and the systematic kinetic study with the most active catalyst (F5PEG) was conducted in a laboratory scale semi batch reactor (Par 4561). Prior to each experiment, the reactor was purged with argon and hydrogen and the catalyst was reduced *in situ* in hydrogen at 120 °C and 5 bar for two hours. Then, a 130 mL solution of xylose in deionized water was saturated with hydrogen in a pre-heating chamber at the experimental temperature and pressure. The aqueous sugar solution was injected into the reactor and two foam catalyst pieces fixed to the agitating shaft functioned as stirrer at 600 rpm.

Liquid-phase samples of about 0.5 mL were withdrawn from the pressurized reactor at different times during the hydrogenation

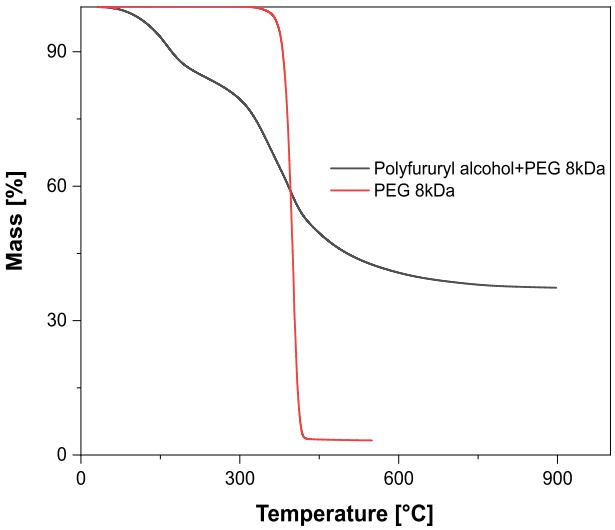

Fig. 1. Thermogravimetric analysis (TGA) of polyfurfuryl alcohol/PEG 8 kDa (5 wt%) mixture and PEG 8 kDa.

experiments, and the concentrations of reactants and products were determined utilizing a high-performance liquid chromatograph (Hitachi Chromaster HPLC) equipped with a Bio-Rad HPX-87C carbohydrate column and a refractive index (RI) detector (Hitachi 5450 RI Detector). The injection volume was 10 μL, and the mobile phase consisted of a 1.2 mM calcium sulphate solution at a flow rate of 0.3 mL/min while the column temperature was maintained at 50 °C.

Minor by-products were identified using gas chromatography (Hewlett Packard G1530AGC) coupled to a mass spectrometer (HP 5973 MSD). Selected samples were lyophilized and mixed with 40 μL of dry pyridine, 160 μL of BSTFA, and 40 μL of TMCS, then oven-dried at 70 °C for about 30 min, after which 5 mL of acetone was added. Finally, 1 μL of the sample was injected into the chromatograph according to the conditions specified by Smeds et al. (2019).

3. Catalyst synthesis results and discussion

A matte gray oxide layer was formed on the Al foams after anodic oxidation and calcination, which agrees with previous observations (Araujo-Barahona et al., 2022; Burgos et al., 2003; Lali et al., 2015a). This treatment resulted in an average mass loss of 7% for all samples.

As described in Section 2.1., the coating of open-cell foam pieces was carried out through the pyrolysis of poly(furfuryl alcohol). The polymerization of furfuryl alcohol proceeded via a stepwise heating process in the presence of an acidic catalyst (oxalic acid). The water in the mixture (evaporating and in liquid phase) plays a critical role in the cross-linking and formation of cavities in the polymer, i.e., the characteristics required to generate adequate cohesion and porosity of the resulting carbon coating (Araujo-Barahona et al., 2022; Cepollaro et al., 2020).

Carbon materials obtained by direct pyrolysis of poly(furfuryl alcohol) are microporous, with nitrogen adsorption–desorption isotherms of type I (Schlumberger and Thommes, 2021), generally with open hysteresis loops due to the limited diffusion of nitrogen molecules in the narrowest nanopores (Cepollaro et al., 2020; Zaharopoulou et al., 2020). Therefore, different activation procedures have been reported to generate mesopores in the carbon structure, such as activation with carbon dioxide and water vapor at high temperatures (Lorenc-Grabowska and Rutkowski, 2018; Sricharoenchaikul et al., 2008), and adding pore formers to the precursor polymer (Lafyatis et al., 1991; Strano et al., 2003). The latter option was considered more feasible because the aluminium in the foams limits the allowed activation temperature.

The attempt to generate mesopores in the carbon framework aligns with the goal of depositing ruthenium nanoparticles with improved dispersion and adsorption of relatively large molecules, because Ru nanoparticles on catalysts supported on carbonaceous materials generally range between 1.5 and 5 nm in size (Aho et al., 2015; Araujo-Barahona et al., 2022; Najarnezhadmashhadi et al., 2020; Sifontes Herrera et al., 2011; Simakova et al., 2016). Hence polyethylene glycol (PEG) with a molar mass of 8 kDa (Lafyatis et al., 1991) was selected.

The carbon resulting from pyrolysis of a mixture of P(FA)/PEG at 550 °C was approximately 40% of the original mass. In contrast, the carbon amount yielded from PEG was almost negligible, as observed in the thermogravimetric measurements shown in Fig. 1 and confirmed by

Table 1
Mass of foam pieces during catalyst synthesis.

Sample Code	PEG Content in Polymer Mixture [wt. %]	Initial Mass [g]	Mass After A.O. [g]	Polymer Loaded [wt. %]	Carbon Mass After Pyrolysis [wt. %]	Carbon Mass After O_2 Activation [wt. %]
F0PEG	0	0.6314 ± 0.0018	0.5915 ± 0.0035	78.90 ± 0.760	59.39 ± 3.67	49.99 ± 7.41
F3PEG	3	0.6179 ± 0.0039	0.5678 ± 0.0054	74.02 ± 1.90	53.25 ± 3.62	32.24 ± 7.33
F5PEG	5	0.6294 ± 0.0017	0.5800 ± 0.0016	64.21 ± 0.11	43.18 ± 0.62	39.06 ± 1.59
F15PEG	15	0.6171 ± 0.0239	0.5705 ± 0.0239	50.94 ± 2.23	29.77 ± 2.20	27.68 ± 2.73

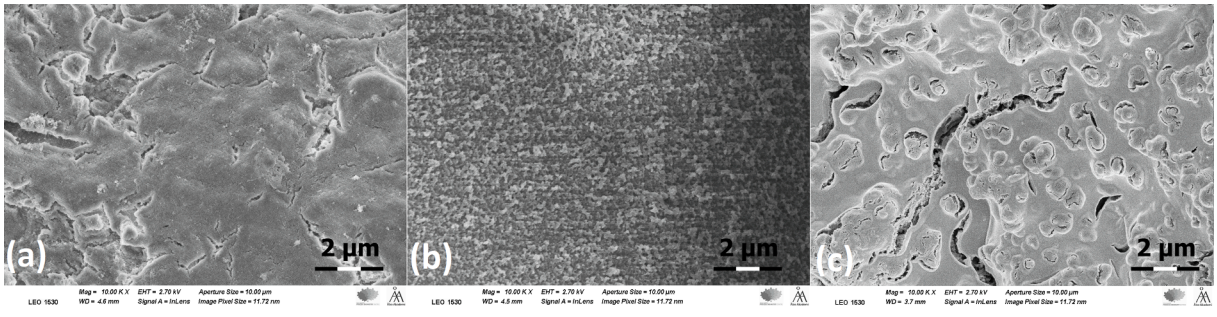

Fig. 2. Effect of PEG (8 kDa) addition on the resulting carbon coatings (SEM images): (a) 0 wt% PEG, (b) 5 wt% PEG, and (c) 15 wt% PEG.

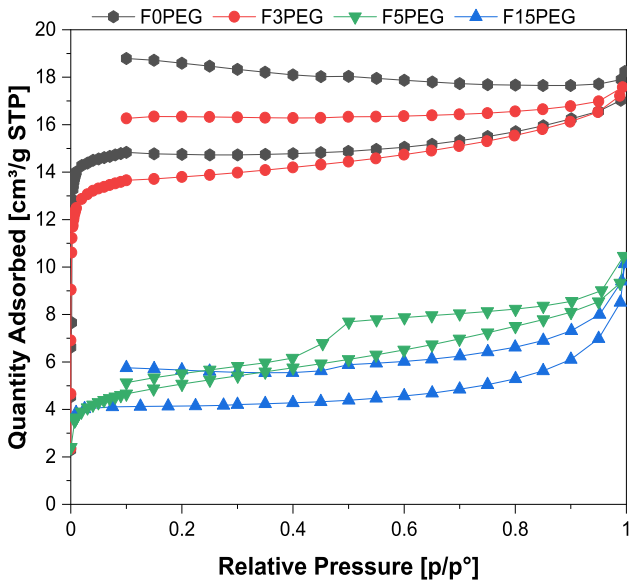

Fig. 3. Nitrogen physisorption isotherms (77 K) recorded for carbon coatings on aluminium foams prepared with different PEG contents in the precursor polymer mixture.

the obtained carbon contents in Table 1. This shows that the selected thermal treatments in the catalyst synthesis (see Section 2.1.) were adequate to completely decompose the pore former (PEG), thus avoiding the possible blockage of ruthenium nanoparticles in the following preparation steps.

Fig. 2 shows the effect of the addition of PEG to the polymer precursor mixture on the resulting carbon coatings. A noticeable increase in the presence of depressions and a more developed porosity were observed with an increasing amount of PEG. However, the carbon layer collapsed when the PEG content exceeded 20 wt%.

The measured nitrogen physisorption isotherms (77 K) for the carbon coatings prepared using different amounts of PEG are presented in Fig. 3, and the derived textural properties are listed in Table 2. For the F0PEG and F3PEG samples, isotherms of type I were obtained with open hysteresis loops, which is characteristic for microporous materials with narrow pores where nitrogen has a limited diffusion capacity at 77 K (Cepollaro et al., 2020; Zaharopoulou et al., 2020). As the PEG content in the precursor polymer mixture increased (i.e., for F5PEG and F15PEG), the resulting isotherms appeared more like type IV isotherms, indicating the presence of mesopores exceeding 4 nm width (Schlumberger and Thommes, 2021).

In fact, the increasing PEG percentage resulted in the formation of mesopores as a result of the collapse of the existing micropores, as can be observed in Figure S1 (Supplementary Information) and Table 2, where the ratio of *meso*-to-micropore volumes increased from the base case of F0PEG with a value of 0.12 up to 1 for F5PEG, the data suggest even the formation of some macroporosity in the sample F15PEG. In contrast, the specific surface area decreased as more mesopores were formed.

Raman spectroscopy is commonly used to characterize pyrolytic carbons (Ferrari and Robertson, 2000), which display a band in the Raman spectra at approximately 1500–1630 cm^{-1}, as well as an additional band located approximately at 1350–1380 cm^{-1} (band D). The G-band is associated to the presence of sp^2 carbon lattices (with E_{2g} vibrational mode), and the D-band is attributed to the A_{1g} vibrational mode, which is Raman-activated due to the presence of small imperfections caused by the loss of translational symmetry in the disordered structure (Li et al., 1996; Wang et al., 1998). Thus, the ratio of the integrated intensities of the D and G Raman bands (I_D/I_G) provides a measure of the degree of disorder in the obtained carbon (Wang et al., 1998).

Fig. 4 shows representative Raman spectra of the carbon-coated foams (F0PEG, F3PEG, and F5PEG) and the calculated I_D/I_G ratio. The spectra were fitted using Gaussian functions. Besides the G and D bands, two additional bands located at 1231 ± 26 cm^{-1} and 1504 ± 3 cm^{-1} were included to achieve an adequate data fitting; these bands have been associated with remaining residues of the pyrolysis process (Zaharopoulou et al., 2020). A slight increase in the I_D/I_G ratio was observed with increasing PEG content; this apparent increase in the disorder can be associated with the destruction of the microcrystalline graphite induced by the presence of PEG that led to a higher degree of burn off during the pyrolysis and oxygen activation steps (Cepollaro et al., 2020; Li et al., 1996; Wang et al., 1998; Zaharopoulou et al., 2020).

Ruthenium nanoparticles were deposited on F0PEG and F5PEG samples to study the effect of the induced mesoporosity of the carbon support on catalytic performance. Under the impregnation conditions described in Section 2.1, Ru loadings of 1.7 wt% for F0PEG and 1.4% for F5PEG were obtained.

The hydrogen-TPR profile for catalyst F5PEG is shown in Fig. 5 (before *ex-situ* reduction), which coincides with the previous results for Ru/C foam catalysts (Araujo-Barahona et al., 2022) (prepared under the conditions of F0PEG), where two hydrogen consumption maxima were observed: the first one at 250 °C is ascribed to the reduction of ruthenium oxides, while the latter was due to methanation of the carbon support, as confirmed by mass spectroscopy. Therefore, 300 °C was used for the *ex-situ* reduction of the prepared catalysts (see Section 2.1).

On the other hand, a better dispersion of Ru was obtained on catalyst F5PEG than on F0PEG (microporous carbon support). The latter had an average nanoparticle size of 3.6 nm, whereas F5PEG had an average size of 2.8 nm, as shown in the TEM micrographs in Fig. 6.

4. Kinetic results and discussion

4.1 Catalyst screening and durability

The mesoporosity introduced in the preparation of F5PEG, confirmed by nitrogen physisorption and SEM images (see Section 3.1), resulted in a higher dispersion of the Ru nanoparticles due to a superior

Table 2
Textural properties of prepared carbon-coated foams.

Sample Code	Dubinin-Radushkevich Specific Surface Area [m^2/g]	BET Specific Surface Area [m^2/g]	Cumulative NLDFT Pore Volume (Pore Width ≤ 50 nm) [cm^3/g]	Cumulative NLDFT Micropores Volume (Pore Width ≤ 2 nm) [cm^3/g]	Cumulative NLDFT Mesopores Volume (Pore Width ≥ 2 nm) [cm^3/g]	Ratio of Meso-to-Micropore Volumes
F0PEG	69	47	0.024	0.021	0.003	0.12
F3PEG	63	46	0.023	0.019	0.004	0.24
F5PEG	20	17	0.012	0.006	0.006	1.00
F15PEG	No fitted	12	0.010	0.005	0.005	0.93

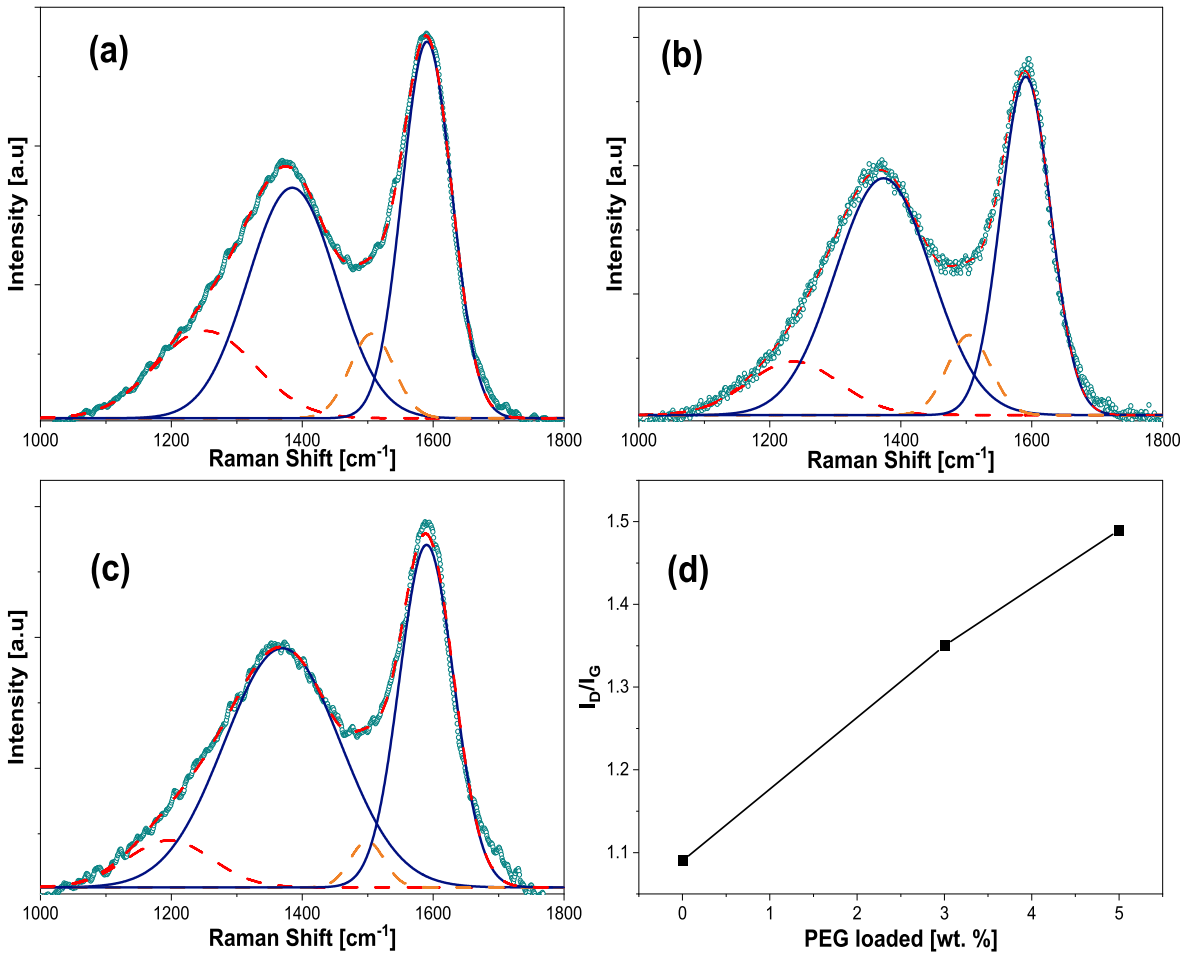

Fig. 4. Raman spectra of the carbon coatings of catalysts (a) F0PEG, (b) F3PEG, (c) F5PEG and (d) ratio between G band and D band versus mass percentage of PEG used in the polymer precursor mixture.

interaction between the ruthenium precursor and the carbon support. Considering that sugar hydrogenation is a structure-sensitive reaction (Simakova et al., 2016), the improved metal dispersion on the mesoporous catalyst F5PEG compared to the purely microporous catalyst F0PEG resulted in higher activity for xylose hydrogenation, as shown in Fig. 7. Consequently, catalyst F5PEG was selected for systematic kinetic experiments and kinetic modelling.

Furthermore, after 200 h of use, a decrease in the catalytic activity of F5PEG was detected in a catalyst recycling experiment (Fig. 8). The primary cause of deactivation was attributed to nanoparticle agglomeration, as shown in Fig. 6 since metal leaching was not detected under the experimental conditions. However, this catalyst retained its activity twice as long compared to purely microporous Ru/C foam catalyst (Araujo-Barahona et al., 2022). This improvement in stability can be attributed to the spatial restriction imposed by the mesopores that contained the metal nanoparticles, preventing their agglomeration, as Cattaneo et al. (2020) have shown for Ru-based catalysts on different carbon supports.

4.2 Results of kinetic experiments

Fig. 9 shows the very strong temperature effect on the reaction rate. The reaction proceeded very slowly at temperatures below 80 °C; however, a considerable enhancement in the hydrogenation rate was observed at temperatures exceeding 100 °C. The selectivity towards xylitol decreased from 99% at lower temperatures (60 °C, 80 °C, and 90

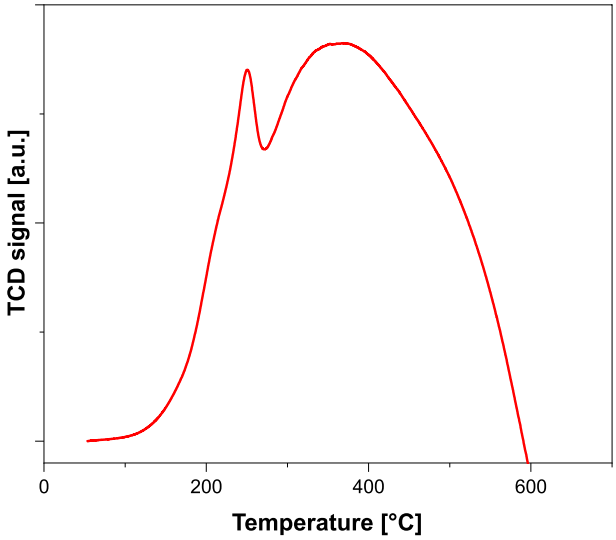

Fig. 5. Hydrogen Temperature-Programmed Reduction (TPR) for catalyst F5PEG. TCD signal = thermal conductivity detector signal.

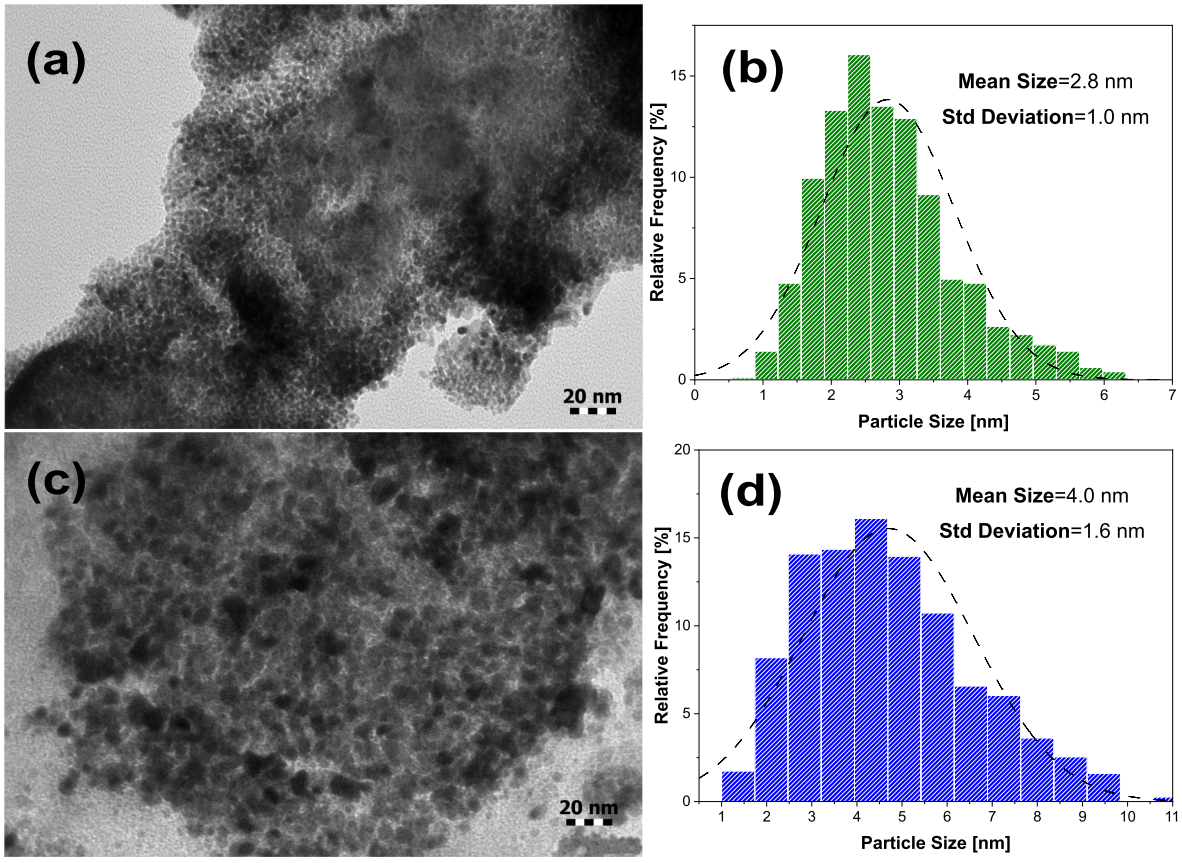

Fig. 6. Ruthenium nanoparticles on catalyst F5PEG: (a) TEM image (fresh catalyst), (b) nanoparticle size distribution (fresh catalyst), (c) TEM image (spent catalyst, 200 h of use), (d) nanoparticle size distribution (spent catalyst, 200 h of use).

°C) to 92% at 120 °C due to the formation of by-products. These observations confirm that the reactions leading to by-product formation have higher activation energies than the main reaction of xylitol formation. Therefore, the selection of the operation temperature for eventual industrial production purposes is an issue of optimizing the productivity and selectivity.

Furthermore, the effect of the hydrogen pressure on the reaction rate was minor, especially for pressures exceeding 50 bar. On the other hand,

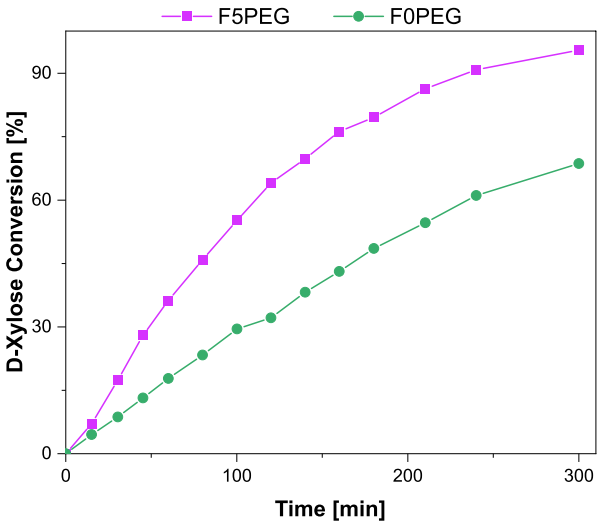

Fig. 7. Comparison of prepared catalysts for the D-xylose hydrogenation at 90 °C and 30 bar of hydrogen pressure.

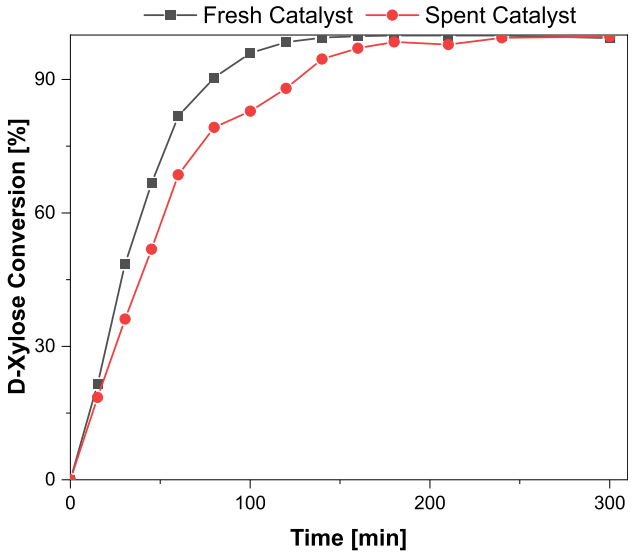

Fig. 8. Decrease of the catalytic activity in F5PEG after 200 h of use in a recycling experiment performed at 100 °C and 40 bar hydrogen pressure.

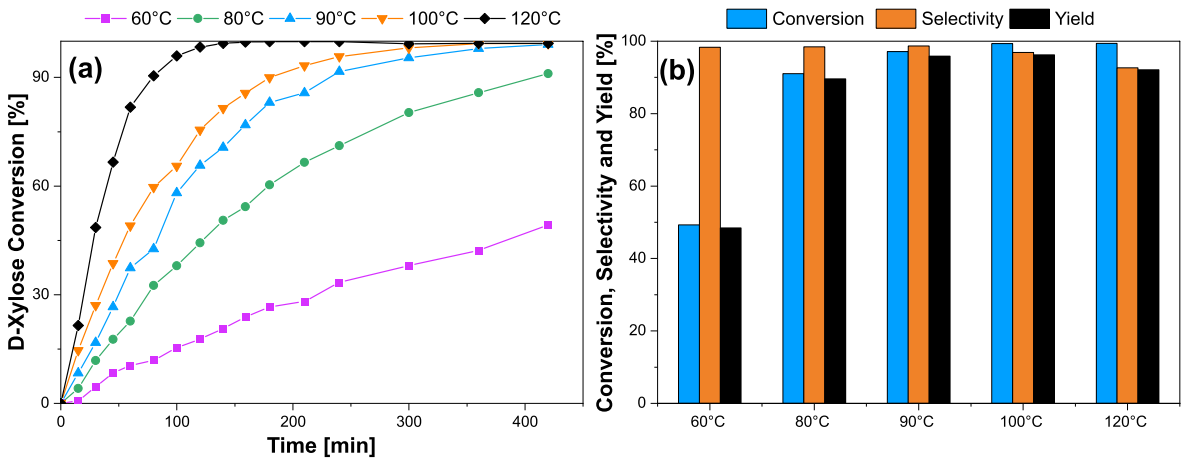

Fig. 9. Effect of temperature at 40 bar hydrogen pressure on (a) the kinetics of D-xylose hydrogenation and (b) conversion, selectivity, and xylitol yield.

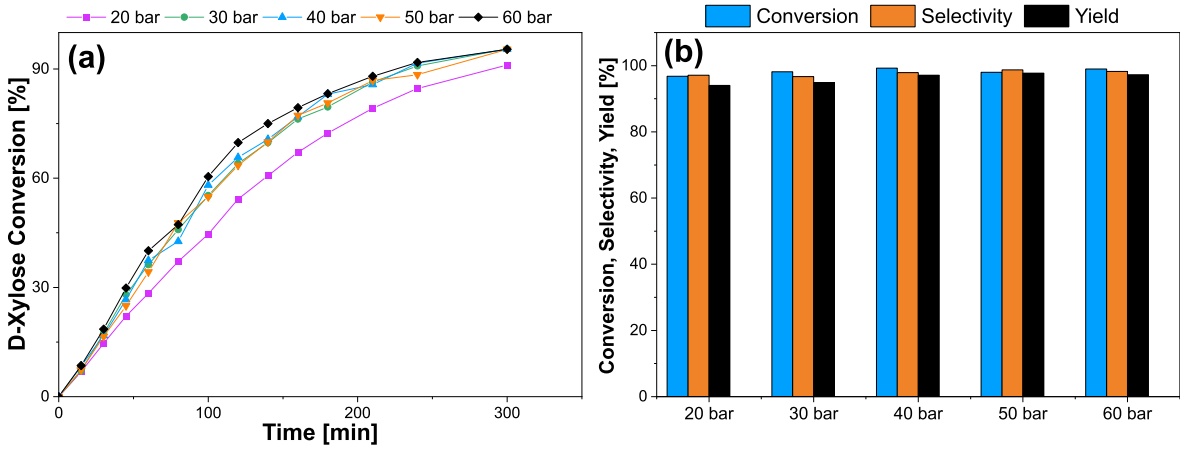

Fig. 10. Effect of the hydrogen pressure at 90 °C on (a) the kinetics of D-xylose hydrogenation and (b) conversion, selectivity, and xylitol yield.

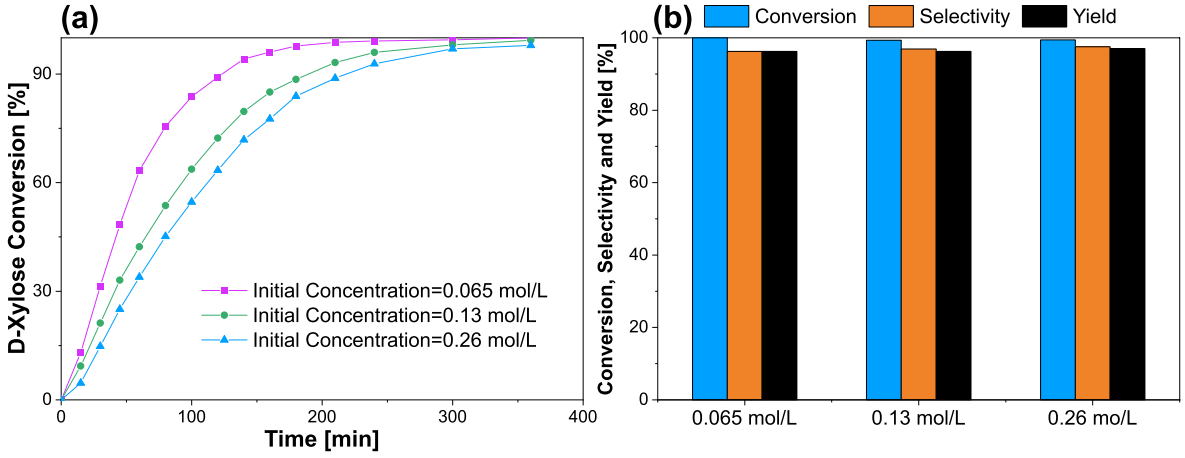

Fig. 11. Effect of the initial D-xylose concentration (40 bar of hydrogen and 100 °C) on (a) the hydrogenation kinetics and (b) conversion, selectivity, and xylitol yield.

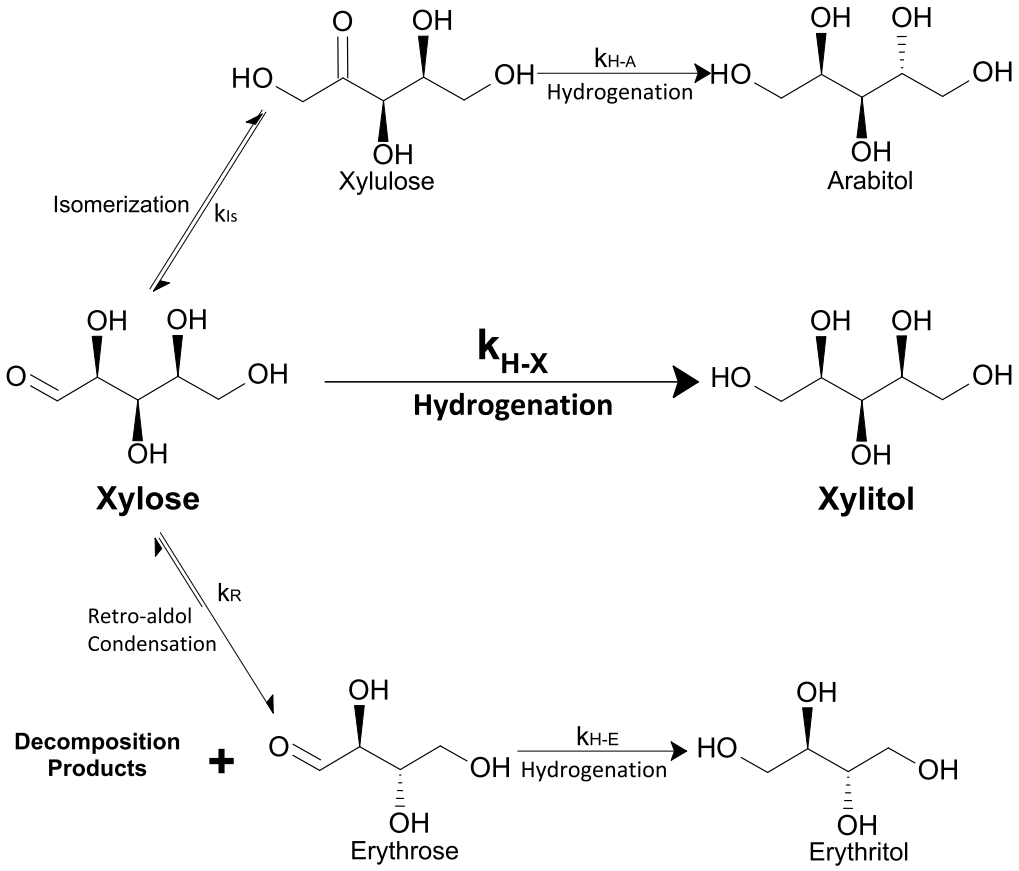

Fig. 12. Proposed reaction scheme for xylose hydrogenation on Ru/C solid foams.

the xylitol selectivity increased slightly with increasing pressure as shown in Fig. 10.

When the effect of the initial concentration of D-xylose was studied an increase in the reaction rate with the decrease in the initial concentration of the sugar was observed as illustrated in Fig. 11. This observation validates that the effective reaction order with respect to xylose is less than 1, indicating the adsorption effect of xylose.

4.3. Reaction stoichiometry and kinetic modelling

4.3.1 Reaction scheme

Fig. 12 shows the proposed reaction scheme based on the identified products with a combination of HPLC and GC–MS (see Supplementary Information). Regardless of the reaction conditions, the by-products did not exceed 2 mol%. The mathematical models developed in this work considered only the main pathway (xylose hydrogenation), as presented in Section 4.3.1.

4.3.2 Kinetic modelling

Fundamental model hypotheses.

The mathematical models developed to describe the experimental data were based on the general hypotheses listed below.

1) The reaction was assumed to proceed within the domain of intrinsic kinetics, i.e., in the absence of internal and external mass transfer limitations, owning to the high agitation speed used during the experiments and the thin catalyst layer on the foam structures. Considering the criterion of Weisz and Hicks (1995) and comparing the diffusion and reaction rates, operation within the kinetic regime was ensured.
2) The system was completely isothermal because of the relatively low value of reaction enthalpy, particularly in case of the low concentrations used (less than0.3 mol/L) during the experiments. Therefore, the energy balance was dismissed.
3) Samples withdrawn from the reactor were less than 6 wt%, so the reaction volume was considered constant during the experiment.
4) As mentioned in Section 4.3.1., the concentration of by-products was minimal. Hence, for the quantitative modelling, it was inferred that the reaction exclusively forms xylitol.
5) The system follows Henry's law, i.e., the concentration of the hydrogen dissolved in the liquid phase is proportional to the hydrogen pressure in the gas phase, as confirmed in a previous study by Sifontes Herrera et al. (2016).
6) Dissociative adsorption of hydrogen was assumed but maintaining its molecular identity in the hydrogenation process—two hydrogen atoms react with the adsorbed sugar.
7) Given the lower adsorption affinity of sugar alcohols (Sifontes Herrera et al., 2011), the adsorption effect of D-xylitol was neglected.
8) Finally, the reaction between the adsorbed sugar molecules and adsorbed hydrogen was assumed to be the rate-determining step of the catalytic process.

As for the mode of adsorption of the reactants on the catalyst surface, three cases were studied: temperature-dependent and temperature-independent non-competitive adsorption, and temperature-independent semi-competitive adsorption. The temperature-dependent

semi-competitive model was discarded to avoid over-parametrization and maintain the reliability of the estimated parameters.

The non-competitive adsorption models assume that due to the size differences between the sugar molecules and hydrogen, it is reasonable to assumed that they are adsorbed on separated active sites. This approach has been applied successfully to describe the hydrogenation of sugars (Mikkola et al., 1999a; Najarnezhadmashhadi et al., 2020), even though it is only an approximation from a physical viewpoint. A modification of this model was included as the second case by considering the effect of temperature on the adsorption parameters. On the other hand, a more realistic model with respect to the mode of adsorption has been proposed by Mikkola et al. (1999a) and Salmi et al. (2004) — the semi-competitive adsorption model. In this case, the larger molecules, i.e., sugar molecules are adsorbed on the primary active sites of the catalyst surface, leaving interstitial sites available for small species, such as hydrogen. The rate equations derived from these hypotheses for each case are discussed in the following section.

5. Model derivation and parameter estimation strategy

5.1. Temperature-independent non-competitive adsorption model

Considering the hypotheses presented, the following surface reaction network was considered, where * represents an active site that adsorbs xylose molecules, while *′ indicates the adsorption sites for hydrogen,

$$X + * \leftrightarrow X*$$

$$H_2 + 2*' \leftrightarrow 2H*'$$

$$X* + 2H*' \rightarrow X_{OH} + * + 2*'$$

The adsorption steps for xylose and hydrogen were assumed to be rapid; therefore, the quasi-equilibrium hypothesis could be applied to these steps, while the third step, the surface reaction, is presumed to be rate-limiting. The total balances of the adsorption sites for hydrogen and xylose were considered in the derivation. Based on these considerations, the final form of the rate equation becomes (a detailed derivation of the rate equation is presented in Supplementary Information)

$$r_X = \frac{\kappa_X \bullet C_X \bullet P_{H_2}}{(1 + K_X \bullet C_X) \bullet \left(1 + \sqrt{K_{H_2} \bullet P_{H_2}}\right)^2} \tag{1}$$

where κ_X is a merged parameter consisting of rate and adsorption parameters. If it is presumed to follow the law of Arrhenius and van't Hoff, the temperature dependence of this parameter can be expressed as in equation (2) for a reference temperature of 90 °C ($\bar{T} = 363\,K$).

$$\kappa_X = \kappa_{X90^\circ C} \bullet e^{\frac{E_A}{R} \bullet \left(\frac{1}{\bar{T}} - \frac{1}{T}\right)} \tag{2}$$

5.2. Temperature-dependent non-competitive adsorption model

On the other hand, if the adsorption parameters of the reactants are temperature-dependent, then they can be expressed by equations (3) and (4), where ΔH_X and ΔH_{H_2} are the adsorption enthalpies of xylose and hydrogen, respectively.

$$K_X = K_{X,\,90^\circ C} \bullet e^{\frac{\Delta H_X}{R} \bullet \left(\frac{1}{\bar{T}} - \frac{1}{T}\right)} \tag{3}$$

$$K_{H_2} = K_{H_2,\,90^\circ C} \bullet e^{\frac{\Delta H_{H_2}}{R} \bullet \left(\frac{1}{\bar{T}} - \frac{1}{T}\right)} \tag{4}$$

5.3. Semi-competitive adsorption model

For the semi-competitive adsorption model, it is assumed that the smaller molecule (hydrogen) occupies one primary site, whereas the larger molecules require m sites for adsorption. Thus, the balance equation for primary sites becomes

$$mC_{*X} + C_{*'H} + C_{*'} = C_0 \tag{5}$$

where C_0 and $C_{*'}$ denote the concentration of vacant sites and the total concentration of primary sites, respectively. The concentration of vacant sites clusters (C_*) is related to the concentration of larger molecules by

$$C_{*X} + C_* = \frac{\alpha \bullet (C_0 - C_{*'H})}{m} \tag{6}$$

Parameter α denotes the maximum coverage of larger molecules ($\alpha \leq 1$). The adsorption quasi-equilibrium hypothesis is applied for hydrogen and xylose and the concentration of vacant primary sites and site clusters are obtained from (see Supplementary Information)

$$C_{*'} = \frac{(1 + (1-\alpha) \bullet K_X \bullet C_X) \bullet C_0}{1 + \sqrt{K_H \bullet C_{H_2}} + \left(1 + (1-\alpha) \bullet \sqrt{K_H \bullet C_{H_2}}\right) \bullet K_X \bullet C_X} \tag{7}$$

The concentration of site clusters is obtained from

$$C_* = \frac{\alpha \bullet C_0}{m \bullet \left(1 + \sqrt{K_H \bullet C_{H_2}} + \left(1 + (1-\alpha) \bullet \sqrt{K_H \bullet C_{H_2}}\right) \bullet K_X \bullet C_X\right)} \tag{8}$$

The rate of the surface reaction is

$$r_X = k_X \bullet C_{*X} \bullet C_{*'H}{}^2 \tag{9}$$

After considering the quasi-equilibria, the expression for the vacant sites phase, and the Henry's law for dissolved hydrogen, the rate expression becomes

$$r_X = \left(\frac{k_X \bullet K_X \bullet K_H \bullet K_{LH_2} \bullet \alpha \bullet C_0{}^3}{m}\right) \bullet \frac{C_X \bullet P_{H_2} \bullet (1 + (1-\alpha) \bullet K_X \bullet C_X)^2}{\left(1 + \sqrt{K_H \bullet K_{LH_2} \bullet P_{H_2}} + \left(1 + (1-\alpha) \bullet \sqrt{K_H \bullet K_{LH_2} \bullet P_{H_2}}\right) \bullet K_X \bullet C_X\right)^3} \tag{10}$$

After introducing the following merged parameters

$$\kappa_X = \frac{k_X \bullet K_X \bullet K_H \bullet K_{LH_2} \bullet C_0{}^3}{m} \tag{11}$$

$$K_{H_2} = K_{LH_2} \bullet K_H \tag{12}$$

the rate equation becomes

$$r_X = \frac{\kappa_X \bullet \alpha \bullet (1 + (1-\alpha) \bullet K_X \bullet C_X)^2 \bullet C_X \bullet P_{H_2}}{\left(1 + \sqrt{K_{H_2} \bullet P_{H_2}} + K_X \bullet C_X + (1-\alpha) \bullet \sqrt{K_{H_2} \bullet P_{H_2}} \bullet K_X \bullet C_X\right)^3} \tag{13}$$

If the parameter κ_X follows the laws of Arrhenius and van't Hoff, being its temperature dependence can be expressed as in equations (2) for a reference temperature of 90 °C ($\bar{T} = 363\,K$).

Table 3
Kinetic parameters estimated for the non-competitive temperature-independent model.

Parameter	Value	Relative Error [%]	Units
$\kappa_{X90^\circ C}$	0.012	5.9	$L \bullet gRu^{-1} \bullet min^{-1}\ bar^{-1}$
E_A	41.77	0.89	$kJ \bullet mol^{-1}$
K_{H_2}	0.072	8.1	bar^{-1}
K_X	9.13	3.8	$L \bullet mol^{-1}$
R^2	98.85	–	%
Q	0.0070	–	$L^2 \bullet mol^{-2}$

Table 4
Correlation matrix for the non-competitive temperature-independent model.

	$\kappa_{X\,90^\circ C}$	E_A	K_{H_2}	K_X
$\kappa_{X\,90^\circ C}$	1	0.0043	0.91	0.18
E_A	0.004	1	−0.055	0.21
K_{H_2}	0.91	−0.055	1	−0.24
K_X	0.18	0.205	−0.24	1

5.3.1. Mass balances for the semibatch reactor

The mass balances of the components in the liquid phase can be written in a very simple manner because all the experiments were carried out in the kinetic regime using a thin catalyst layer and high stirring speed, thus avoiding the appearance of concentration gradients in the system. Equations (14) and (15) describe the mass balances for xylose and xylitol, respectively, where ρ_B is the bulk density ($\rho_B = \frac{m_{cat}}{V_L}$). The mass balance of hydrogen is omitted because the reactor operated under constant pressure.

$$\frac{dC_X}{dt} = -r_X \bullet \rho_B \tag{14}$$

$$\frac{dC_{X_{OH}}}{dt} = r_X \bullet \rho_B \tag{15}$$

The model was solved in Python by minimizing the objective function presented in equation (16) with the Nelder-Mead optimization method. The LSODA solver was employed for the numerical solution of the ordinary differential equations (14) and (15).

$$Q = \sum_{i=1}^{n} \left(C_{Exp,i} - C_{Calc,i}\right)^2 \tag{16}$$

5.4 Modelling results and discussion

5.4.1 Non-competitive adsorption models – Temperature effect

The non-competitive adsorption model was solved for the two cases described in the previous section, i.e., considering the adsorption parameters as temperature-independent and dependent. Table 3 lists the parameters obtained for the temperature independent case. As expected, the model provides a high degree of explanation and describes rather well the concentration profiles of reactants and products, and the values of the parameters match our previous results for the hydrogenation of monomeric sugars (Araujo Barahona et al., 2022).

Furthermore, a low degree of correlation between the estimated parameters was obtained, as shown in Table 4. The highest Pearson correlation coefficient was obtained for parameters $\kappa_{X\,90^\circ C}$ and k_{H_2}.

Although this model described the kinetic data satisfactorily, the results obtained with the model that considers reactant adsorption as a process affected by temperature improved the overall description of the experimental results. The estimated parameters are listed in Table 5. This approach yielded a higher degree of explanation (R^2) and a lower value for the objective function (Q), as well as a suppressed correlation between the parameters, as reported in Table 6, yielding values of the Pearson correlation coefficient of less than 0.5 in all cases.

Fig. 13 shows the fitting results for the temperature-dependent adsorption model, demonstrating how this model very successfully predicts the effect of temperature on the hydrogenation process. The deviations observed at high conversion values, especially at 120 °C, can be ascribed to the minor formation of by-products.

Figs. 14 and 15 confirm that the proposed model predicted very satisfactorily the effect of the hydrogen pressure and the initial concentrations of xylose on the reaction kinetics, respectively.

In addition, the parity plot displayed in Fig. 16 shows good agreement between the concentrations predicted by the selected model and the experimental data, with an overall deviation lower than 10%.

Remarkably, the temperature-dependent adsorption model predicts

Table 5
Kinetic parameters estimated for the non-competitive temperature-dependent model.

Parameter	Value	Relative Error [%]	Units
$\kappa_{X\,90^\circ C}$	0.012	0.43	$L \bullet gRu^{-1} \bullet min^{-1}\ bar^{-1}$
E_A	20.20	1.8	$kJ \bullet mol^{-1}$
$k_{H_2,90^\circ C}$	0.073	0.27	bar^{-1}
$k_{X,90^\circ C}$	8.38	0.20	$L \bullet mol^{-1}$
ΔH_X	−18.80	0.20	$kJ \bullet mol^{-1}$
ΔH_{H_2}	39.22	0.20	$kJ \bullet mol^{-1}$
R^2	99.07	–	%
Q	0.0057	–	$L^2 \bullet mol^{-2}$

that xylose adsorption is an endothermic process, that is, the adsorption of this sugar increases with increasing temperature, which is superficially inconsistent with the conventional thermodynamic viewpoint. Crezee et al. (2003) reported similar results when modeling kinetic data for the hydrogenation of glucose on Ru/C catalysts and hypothesized that the adsorption of D-glucose proceeds via the formation of an anionic intermediate derived from the ring form of the molecule that is attacked by hydride-like ruthenium species on the catalyst surface. Hence, the endothermic character of the adsorption process reflected by the estimated parameters may be a consequence of the complex adsorption mode.

Mikkola et al. (1999b) have shown through NMR spectrometric studies that in aqueous solutions, xylose co-exists mainly as a mixture of α-xylopyranose and β-xylopyranose. The equilibrium between the α/β forms with respect to temperature was S-shaped, with the α-form being favored with increasing temperature. Because all the species present in the mixture would have different reactivities and adsorption affinities, xylose adsorption is a complex process that is also affected by temperature and other factors, such as the pH of the mixture.

5.4.2 Semi-competitive adsorption model

The mode of adsorption of sugar molecules and hydrogen was studied by fitting the semi-competitive model which considers that the larger carbohydrate molecules are adsorbed in the primary sites in such a way that interstitial sites remain accessible mainly for hydrogen. Table 7 shows that the competitiveness factor is $\alpha = 0.74$. The modelling results indicate that maximally about 70% of the primary adsorption sites on the ruthenium surface can be occupied by the sugar molecules. Between the adsorbed sugar molecules, some interstitial sites remain thus available for hydrogen adsorption, which is reasonable, considering the size differences between the sugar molecules and hydrogen. For the idealized case of spherical molecules (with radius R) organized on a flat surface, the ratio between the area occupied by the molecules and the total area is $\pi R^2/(2R)^2 = \pi/4 = 0.785$ for a rectangular arrangement and $\pi/(2\sqrt{3}) = 0.907$ for a triangular arrangement, which can be regarded as the limit values.

The adsorption coefficient of xylose is much higher than that of hydrogen in the models considered here. One way to confirm this observation might be to separately measure the sugar adsorption on ruthenium. However, it is not in reality possible to determine the adsorption coefficient of xylose in separate experiments, because the catalyst would be deactivated if it is exposed to xylose at elevated temperatures in the absence of hydrogen. Furthermore, the total (overall) adsorption coefficient of xylose might not reflect the reaction conditions, because only a fraction of the adsorption sites is active in heterogeneous catalysis. In general, it can be concluded that the value of the sugar adsorption coefficient was of the same order of magnitude as reported previously. The adsorption coefficient of arabinose was 8.8 L/mol in a previous study (Araujo Barahona et al., 2022), which is very comparable with the values reported for xylose in Tables 3, 5, and 7. The activation energy was relatively high, which is in accordance with the

Table 6
Correlation matrix for the non-competitive temperature-dependent model.

	$\kappa_{X90^\circ C}$	E_A	$k_{H_2,90^\circ C}$	$k_{X,90^\circ C}$	ΔH_X	ΔH_{H_2}
$\kappa_{X90^\circ C}$	1	−0.25	0.48	0.20	0.0036	−0.0029
E_A	−0.25	1	−0.10	−0.034	−0.0082	−0.0194
$k_{H_2,90^\circ C}$	0.48	−0.10	1	−0.0042	−0.0042	0.0099
$k_{X,90^\circ C}$	0.20	−0.034	−0.0042	1	0.0111	0.014
ΔH_X	0.0036	−0.0082	−0.0042	0.0111	1	−0.0068
ΔH_{H_2}	−0.0029	−0.019	0.0099	0.014	−0.0068	1

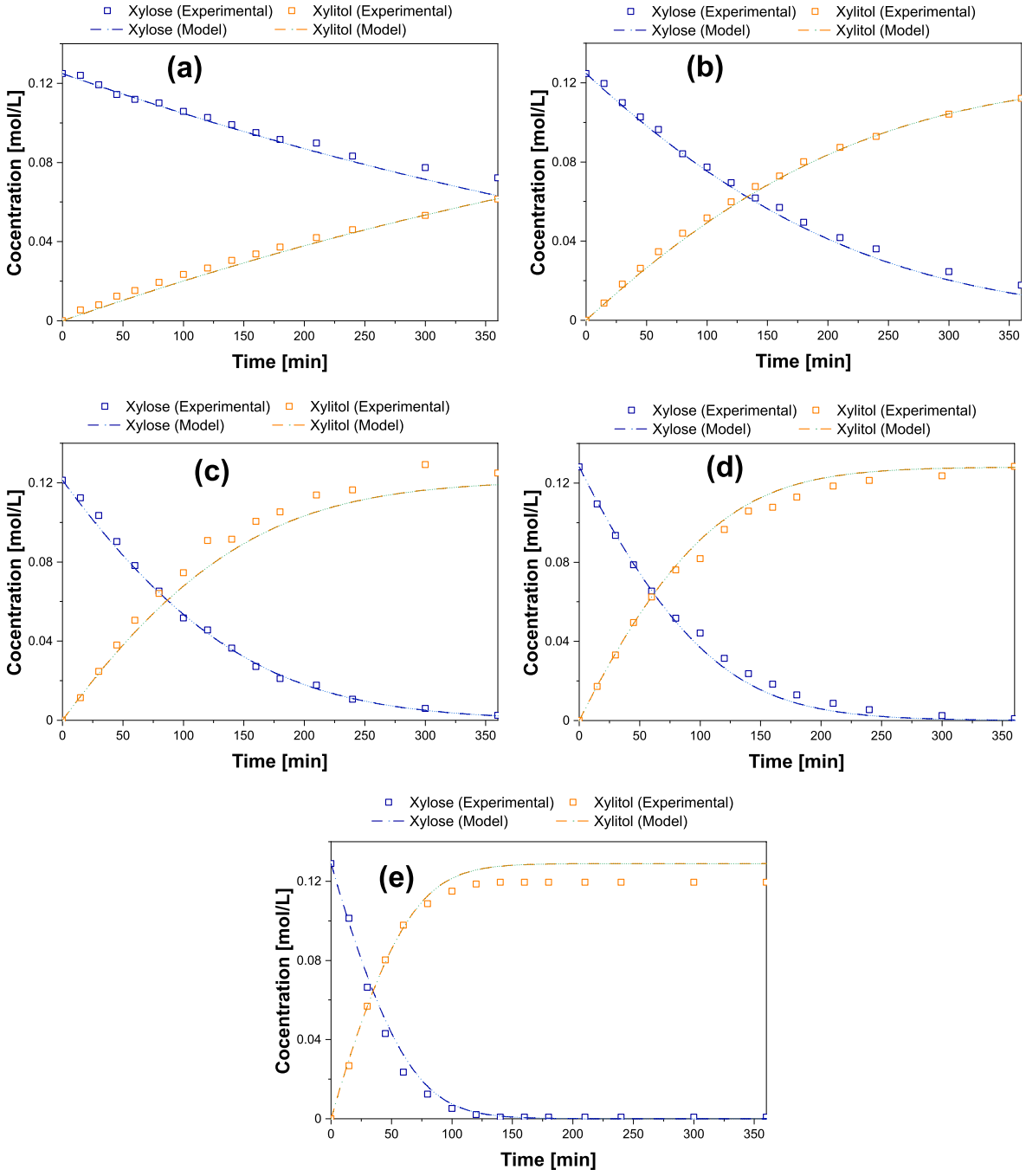

Fig. 13. Modeling D-xylose hydrogenation at 40 bar and (a) 60℃, (b) 80℃, (c) 90 ℃, (d) 100 ℃, and (e) 120 ℃ using the non-competitive temperature-dependent adsorption model.

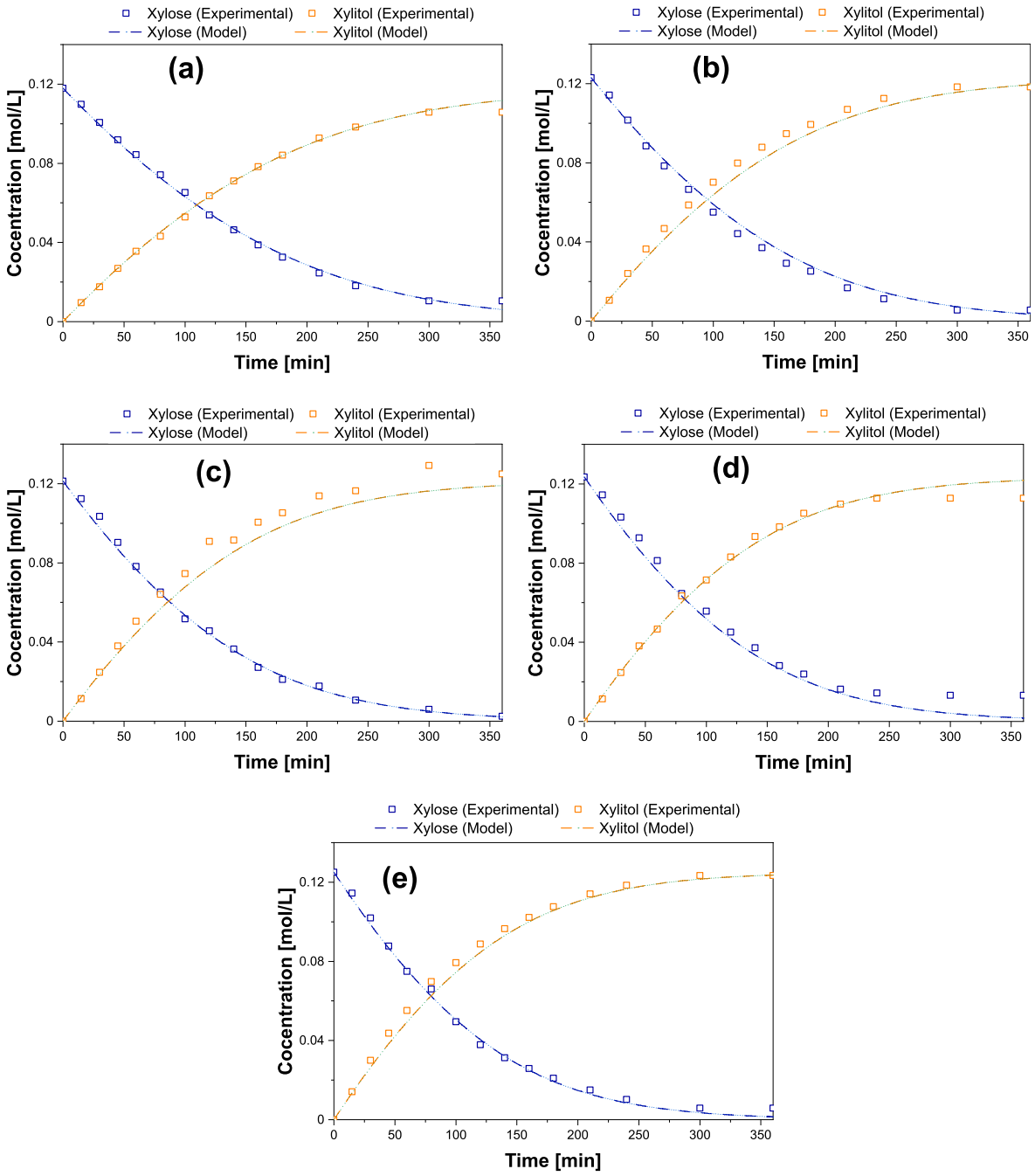

Fig. 14. Modeling D-xylose hydrogenation at 90℃ and (a) 20 bar, (b) 30 bar, (c) 40 bar, (d) 50 bar, and (e) 60 bar using the non-competitive temperature-dependent adsorption model.

primary data displayed in Fig. 9, where is evident that reaction rate was strongly dependent on temperature.

A high degree of explanation and low value of the objective function were achieved in the parameter estimation. In terms of the reliability of the obtained parameters, in all cases, Pearson correlation values less than 0.5 were obtained, as shown in Table 8.

To explore the effect of changing the competitiveness factor on the overall performance of the model, the value of α was varied between 0.1 and 1, while the other parameters were fixed to the values obtained from the regression analysis. The simulation results are shown in Fig. 17. As can be observed, the fraction of active sites maximally occupied by sugar molecules seems to be well defined within the value of 0.74.

Additionally, when the value of the competitiveness factor is allowed to float between 0.1 and 1, the standard errors of the estimated parameters and the degree of correlation between them increase (see Supplementary Information). This is expected because the semi-competitive model provides a more realistic approximation of the distribution of the reactants on the active sites during the catalytic process compared to the extreme cases of non-competitive and competitive adsorption ($\alpha = 1$).

6. Conclusions and future perspectives

The properties of the carbon coating obtained by the pyrolysis of

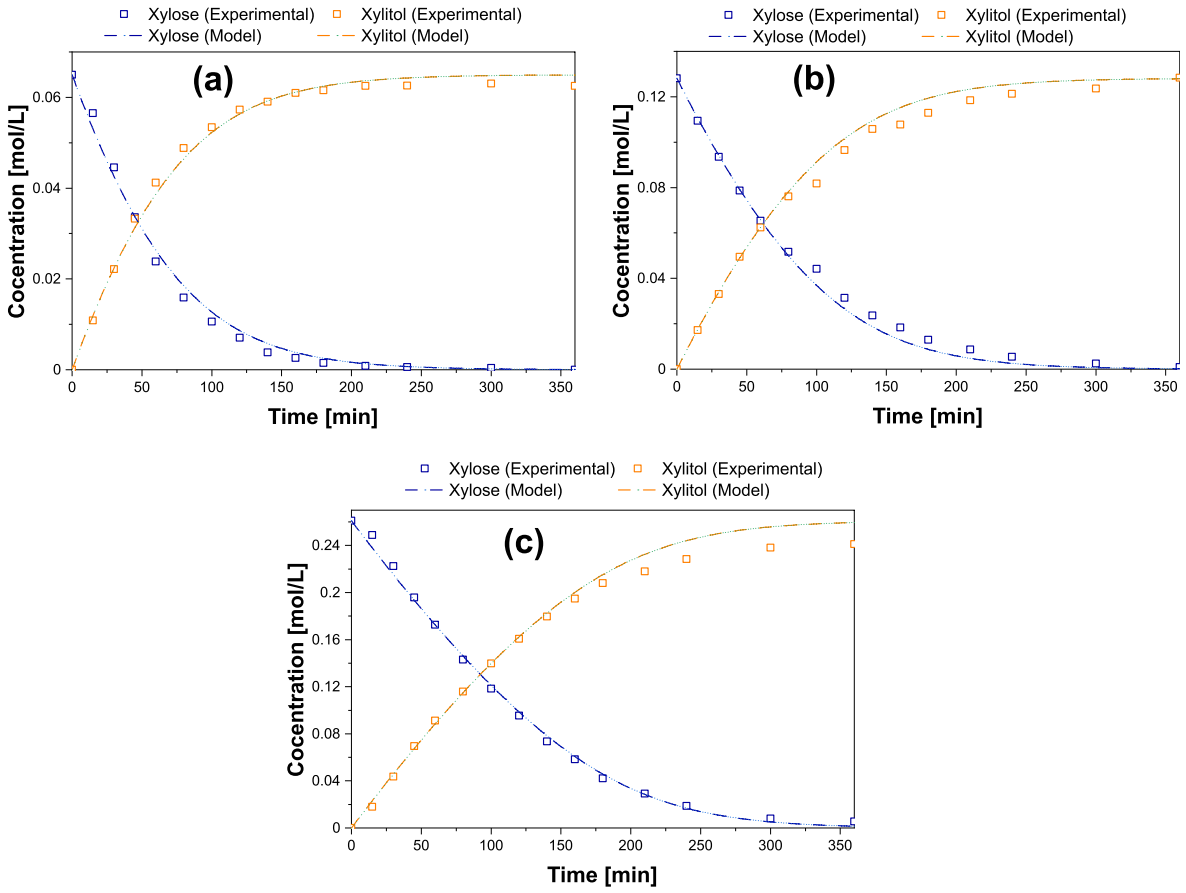

Fig. 15. Modeling D-xylose hydrogenation at 100℃ and 40 bar of hydrogen pressure, with an initial concentration of (a) 0.06 mol/L, (b) 0.13 mol/L, and (c) 0.26 mol/L (non-competitive temperature-dependent adsorption model).

poly(furfuryl alcohol) in the preparation of Ru/C solid foam catalysts were successfully tuned by adding polyethylene glycol (PEG 8 kDa) as a pore former, resulting in the case of 5 wt% PEG (F5PEG), a carbon coating with a ratio of *meso*-to-micropore volumes equal to unity. The induced mesoporosity resulted in better dispersion of the ruthenium nanoparticles because of the higher interaction between the ruthenium precursor and the carbon support. In addition, the F5PEG catalyst exhibited two-fold stability compared to the microporous carbon obtained in the absence of PEG owing to the spatial restriction induced by the mesopores that contain the ruthenium nanoparticles and prevent their agglomeration.

The most active of the prepared catalysts (F5PEG) was used in an

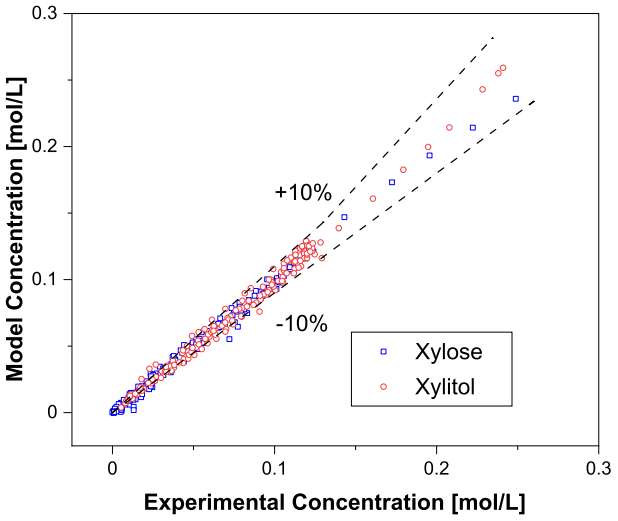

Fig. 16. Parity plot for the modelling results of D-xylose hydrogenation with the non-competitive temperature-dependent model.

Table 7
Kinetic parameters estimated for the semi-competitive adsorption model.

Parameter	Value	Relative Error [%]	Units
$\kappa_{X90^\circ C}$	0.041	0.30	L•gRu^{-1}•min^{-1} mol^{-1}
E_A	42.08	0.15	kJ•mol^{-1}
K_{H_2}	0.035	0.38	bar^{-1}
K_X	5.17	0.15	L•mol^{-1}
α	0.740	0.15	Adimensional
R^2	98.90	–	%
Q	0.0072	–	L^2•mol^{-2}

Table 8
Correlation matrix for the semi-competitive adsorption model.

	$\kappa_{X90^\circ C}$	E_A	K_{H_2}	K_X	α
$\kappa_{X90^\circ C}$	1	−0.029	0.41	0.081	−0.14
E_A	−0.029	1	0.025	0.007	−0.009
K_{H_2}	0.412	0.025	1	−0.070	0.110
K_X	0.081	0.007	−0.070	1	0.024
α	−0.144	−0.009	0.11	0.024	1

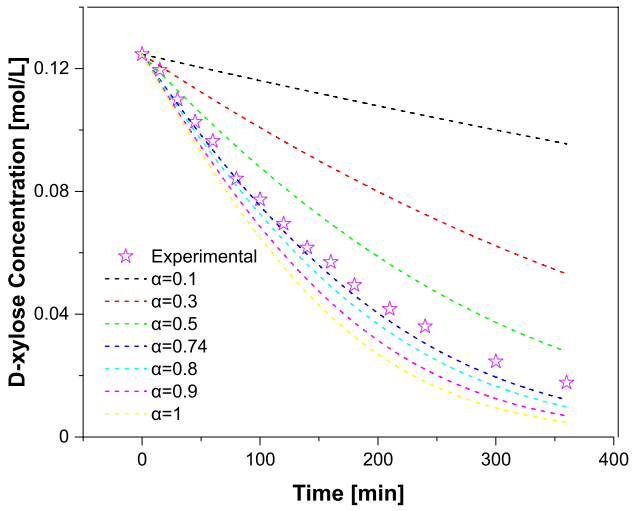

Fig. 17. Effect of varying the competitiveness factor value (α) in the semi-competitive adsorption model applied to a D-xylose hydrogenation experiment at 40 bar and 80℃.

extensive kinetic study of the selective hydrogenation of xylose to xylitol. The effects of temperature, hydrogen pressure, and initial concentration on the reaction rate and product distribution were evaluated. The kinetic data were successfully described using a mathematical model based on the hypothesis of non-competitive adsorption of sugars and hydrogen. Two variations of the model were investigated: one that considers the effect of temperature on the adsorption parameters and a simplified one ignoring this effect. In general, better performance was obtained with the first model in terms of fit and reliability of the obtained parameters. The model predicts that xylose adsorption is an endothermic process. The confirmed experimental observation reveals that the adsorption of sugars on ruthenium surfaces is a complex process since monomeric sugars, such as xylose, exist as a mixture of different species in aqueous solutions; they all have different reactivities and adsorption affinities influenced by the reaction temperature.

The adsorption mode of xylose and hydrogen was studied through the implementation of a semi-competitive model based on the assumption that larger molecules, such as sugars, are adsorbed on the primary active sites of the catalyst in such a way that interstitial active sites remain accessible for smaller species such as hydrogen. The resulting value for the competitiveness factor was$\alpha = 0.74$, indicating, as expected, that the model predicts that most of the active sites can be covered by the larger molecules. Furthermore, the fitting tests revealed that this value is well-defined and provides a more realistic approximation of the distribution of the molecules on the catalyst surface compared with the extreme cases of non-competitive and competitive adsorption.

This study was performed in a vigorously stirred semibatch reactor to measure and model the intrinsic kinetics of xylose hydrogenation. In fact, we have started investigations in a continuous three-phase reactor to screen reaction conditions, such as flow rates, temperature, and concentration levels. Experiments in the continuous reactor system can also provide information on the long-term stability of the catalyst. The final goal is to provide a process concept for continuous sugar hydrogenation on solid foam catalysts.

Declaration of Competing Interest

The authors declare that they have no known competing financial interests or personal relationships that could have appeared to influence the work reported in this paper.

Data availability

Data will be made available on request.

Acknowledgements

This work is part of the activities financed by the Academy of Finland through the Academy Professor's grants 319002, 320115, 345053 (T. Salmi). Economic support from Åbo Akademi University Graduate School (G. Araujo-Barahona) is gratefully acknowledged. J. García-Serna thanks the Agencia Estatal de Investigación and FEDER Funds EU for funding project reference PID2019-105975 GB-I00 (MICINN/FEDER, EU), TED2021-129837B-C42 (I00 (MICINN/FEDER, EU Next-Generation), and Junta de Castilla y León—Consejería de Educación and FEDER Funds project reference CLU-2019-04. Authors thank the Electron Microscopy Laboratory, Institute of Biomedicine, University of Turku, and Biocenter Finland.

Appendix A. Supplementary data

Supplementary data to this article can be found online at https://doi.org/10.1016/j.ces.2023.119130.

References

Aguilar, D.L., Rodríguez-Jasso, R.M., Zanuso, E., de Rodríguez, D.J., Amaya-Delgado, L., Sanchez, A., Ruiz, H.A., 2018. Scale-up and evaluation of hydrothermal pretreatment in isothermal and non-isothermal regimen for bioethanol production using agave bagasse. Bioresour Technol 263, 112–119.

Aho, A., Roggan, S., Eränen, K., Salmi, T., Murzin, D.Y., 2015. Continuous hydrogenation of glucose with ruthenium on carbon nanotube catalysts. Catal Sci Technol 5 (2), 953–959.

Ajao, O., Marinova, M., Savadogo, O., Paris, J., 2018. Hemicellulose based integrated forest biorefineries: Implementation strategies. Ind Crops Prod 126, 250–260.

Akpe, S.G., Choi, S.H., Ham, H.C., 2021. Conversion of cyclic xylose into xylitol on Ru, Pt, Pd, Ni, and Rh catalysts: A density functional theory study. Physical Chemistry Chemical Physics 23 (46), 26195–26208.

Araujo Barahona, G., Eränen, K., Murzin, D., García Serna, J., Salmi, T., 2022. Reaction mechanism and intrinsic kinetics of sugar hydrogenation to sugar alcohols on solid foam Ru/C catalysts – From arabinose and galactose to arabitol and galactitol. Chem Eng Sci 254, 117627. https://doi.org/10.1016/J.CES.2022.117627.

Araujo-Barahona, G., Eränen, K., Oña, J.P., Murzin, D., García-Serna, J., Salmi, T., 2022. Solid Foam Ru/C Catalysts for Sugar Hydrogenation to Sugar Alcohols-Preparation, Characterization, Activity, and Selectivity. Ind Eng Chem Res 61, 2734–2747. https://doi.org/10.1021/ACS.IECR.1C04501.

Autio, J.T., 2002. Effect of xylitol chewing gum on salivary streptococcus mutans in preschool children. J Dent Child 69.

Burgos, N., Paulis, M., Montes, M., 2003. Preparation of Al_2O_3/Al monoliths by anodisation of aluminium as structured catalytic supports. J Mater Chem 13 (6), 1458.

Cattaneo, S., Stucchi, M., Veith, G.M., Prati, L., Wang, D.i., Wang, W.u., Villa, A., 2020. Ru supported on micro and mesoporous carbons as catalysts for biomass-derived molecules hydrogenation. Catal Today 357, 143–151.

Cepollaro, E.M., Caputo, D., Cimino, S., Gargiulo, N., Lisi, L., 2020. Synthesis and Characterization of Activated Carbon Foam from Polymerization of Furfuryl Alcohol Activated by Zinc and Copper Chlorides. C — Journal of Carbon Research 6, 45. https://doi.org/10.3390/c6030045.

Crezee, E., Hoffer, B.W., Berger, R.J., Makkee, M., Kapteijn, F., Moulijn, J.A., 2003. Three-phase hydrogenation of D-glucose over a carbon supported ruthenium catalyst - Mass transfer and kinetics. Appl Catal A Gen 251. https://doi.org/10.1016/S0926-860X(03)00587-8.

Delgado Arcaño, Y., Valmaña García, O.D., Mandelli, D., Carvalho, W.A., Magalhães Pontes, L.A., 2020. Xylitol: A review on the progress and challenges of its production by chemical route. Catal Today 344, 2–14.

Erramouspe, J., Heyneman, C.A., 2000. Treatment and prevention of otitis media. Annals of Pharmacotherapy 34 (12), 1452–1468.

Ferrari, A.C., Robertson, J., 2000. Interpretation of Raman spectra of disordered and amorphous carbon. Phys Rev B Condens Matter Mater Phys 61 (20), 14095–14107.

Ho, P.H., Ambrosetti, M., Groppi, G., Tronconi, E., Palkovits, R., Fornasari, G., Vaccari, A., Benito, P., 2019. Structured Catalysts-Based on Open-Cell Metallic Foams for Energy and Environmental Applications. In: in: Studies in Surface Science and Catalysis. https://doi.org/10.1016/B978-0-444-64127-4.00015-X.

Hoffer, B.W., Crezee, E., Mooijman, P.R.M., van Langeveld, A.D., Kapteijn, F., Moulijn, J. A., 2003. Carbon supported Ru catalysts as promising alternative for Raney-type Ni in the selective hydrogenation of d-glucose. Catalysis Today 79-80, 35–41.

Italiano, C., Ashraf, M.A., Pino, L., Quintero, C.W.M., Specchia, S., Vita, A., 2018. Rh/CeO_2 thin catalytic layer deposition on alumina foams: Catalytic performance and controlling regimes in biogas reforming processes. Catalysts 8 (10), 448.

Kandelman, D., 1997. Sugar, alternative sweeteners and meal frequency in relation to caries prevention: new perspectives. British Journal of Nutrition 77 (S1), S121–S128.
Lafyatis, D.S., Tung, J., Foley, H.C., 1991. Poly(furfuryl alcohol)-Derived Carbon Molecular Sieves: Dependence of Adsorptive Properties on Carbonization Temperature, Time, and Poly(ethylene glycol) Additives. Ind Eng Chem Res 30 (5), 865–873.
Lali, F., Böttcher, G., Schöneich, P.-M., Haase, S., Hempel, S., Lange, R., 2015a. Preparation and characterization of Pd/Al2O3 catalysts on aluminum foam supports for multiphase hydrogenation reactions in rotating foam reactors. Chemical Engineering Research and Design 94, 365–374.
Lali, F., Gärtner, S., Haase, S., Lange, R., 2015b. Preparation Method for Ruthenium Catalysts Supported by Carbon-Coated Aluminum Foams. Chem Eng Technol 38 (8), 1353–1361.
Li, G., Lu, Z., Huang, B., Wang, Z., Huang, H., Xue, R., Chen, L., 1996. Raman scattering investigation of carbons obtained by heat treatment of a polyfurfuryl alcohol. Solid State Ion 89. https://doi.org/10.1016/0167-2738(96)00352-9.
Lorenc-Grabowska, E., Rutkowski, P., 2018. Tailoring mesoporosity of poly(furfuryl alcohol)-based activated carbons and their ability to adsorb organic compounds from water. J Mater Cycles Waste Manag 20 (3), 1638–1647.
Mäkinen, K.K., Olak, J., Russak, S., Saag, M., Seedre, T., Vasar, R., Vihalemm, T., Mikelsaar, M., Mäkinen, P.-L., 1998. Polyol-combinant saliva stimulants: A 4-month pilot study in young adults. Acta Odontol Scand 56 (2), 90–94.
Mariscal, R., Maireles-Torres, P., Ojeda, M., Sádaba, I., López Granados, M., 2016. Furfural: A renewable and versatile platform molecule for the synthesis of chemicals and fuels. Energy Environ Sci 9 (4), 1144–1189.
Mattila, P.T., Svanberg, M.J., Mäkinen, K.K., Knuuttila, M.L.E., 1996. Dietary xylitol, sorbitol and D-mannitol but not erythritol retard bone resorption in rats. Journal of Nutrition 126.
Medek, Jiří, 1977. Possibility of micropore analysis of coal and coke from the carbon dioxide isotherm. Fuel 56 (2), 131–133.
Mikkola, J.P., Salmi, T., Sjöholm, R., 1999a. Modelling of kinetics and mass transfer in the hydrogenation of xylose over Raney nickel catalyst. Journal of Chemical Technology and Biotechnology 74. https://doi.org/10.1002/(SICI)1097-4660(199907)74:7<655::AID-JCTB96>3.0.CO;2-G.
Mikkola, J.-P., Sjöholm, R., Salmi, T., Mäki-Arvela, P., 1999b. Xylose hydrogenation: Kinetic and NMR studies of the reaction mechanisms. Catal Today 48 (1-4), 73–81.
Mitchell, H., 2007. Sweeteners and Sugar Alternatives in Food Technology. Sweeteners and Sugar Alternatives in Food Technology. https://doi.org/10.1002/9780470996003.
Moreno-Castilla, C., Mahajan, O.P., Walker, P.L., Jung, H.-J., Vannice, M.A., 1980. Carbon as a support for catalysts-III glassy carbon as a support for iron. Carbon N Y 18 (4), 271–276.
Murzin, D.Y., Duque, A., Arve, K., Sifontes, V., Aho, A., Eränen, K., Salmi, T., 2016. Catalytic hydrogenation of sugars, in: RSC Green Chemistry. https://doi.org/10.1039/9781782622079-00089.
Najarnezhadmashhadi, A., Eränen, K., Engblom, S., Aho, A., Murzin, D., Salmi, T., 2020. Continuous Hydrogenation of Monomeric Sugars and Binary Sugar Mixtures on a Ruthenium Catalyst Supported by Carbon-Coated Open-Cell Aluminum Foam. Ind Eng Chem Res 59 (30), 13450–13459.
Redina, E., Tkachenko, O., Salmi, T., 2022. Recent Advances in C5 and C6 Sugar Alcohol Synthesis by Hydrogenation of Monosaccharides and Cellulose Hydrolytic Hydrogenation over Non-Noble Metal Catalysts. Molecules 27 (4), 1353.
Research and Markets, 2021a. Global Xylitol Market By Form (Powder and Liquid), By Application (chewing gum, confectionery, bakery & other foods, oral care, and others). By Regional Outlook, Industry Analysis Report and Forecast, pp. 2021–2027.
Research and Markets, 2021b. Xylitol Market: Global Industry Trends. Share, Size, Growth, Opportunity and Forecast 2022–2027.
Ruppert, A.M., Weinberg, K., Palkovits, R., 2012. Hydrogenolysis goes bio: From carbohydrates and sugar alcohols to platform chemicals. Angewandte Chemie - International Edition 51 (11), 2564–2601.
Salmi, T., Murzin, D.Y., Mikkola, J.-P., Wärnå, J., Mäki-Arvela, P., Toukoniitty, E., Toppinen, S., 2004. Advanced kinetic concepts and experimental methods for catalytic three-phase processes. Ind Eng Chem Res 43 (16), 4540–4550.
Sapunov, V.N., Grigoryev, M.Y., Sulman, E.M., Konyaeva, M.B., Matveeva, V.G., 2013. D-glucose hydrogenation over Ru nanoparticles embedded in mesoporous hypercrosslinked polystyrene. Journal of Physical Chemistry A 117. https://doi.org/10.1021/jp312703j.
Schimpf, S., Bron, M., Claus, P., 2004. Carbon-coated microstructured reactors for heterogeneously catalyzed gas phase reactions: Influence of coating procedure on catalytic activity and selectivity. Chemical Engineering Journal 101 (1-3), 11–16.
Schlumberger, C., Thommes, M., 2021. Characterization of Hierarchically Ordered Porous Materials by Physisorption and Mercury Porosimetry—A Tutorial Review. Adv Mater Interfaces 8 (4), 2002181.
Sifontes Herrera, V.A., Oladele, O., Kordás, K., Eränen, K., Mikkola, J.-P., Murzin, D.Y., Salmi, T., 2011. Sugar hydrogenation over a Ru/C catalyst. Journal of Chemical Technology and Biotechnology 86 (5), 658–668.
Sifontes Herrera, V.A., Rivero Mendoza, D.E., Leino, A.R., Mikkola, J.P., Zolotukhin, A., Eränen, K., Salmi, T., 2016. Sugar hydrogenation in continuous reactors: From catalyst particles towards structured catalysts. Chemical Engineering and Processing - Process Intensification 109, 1–10. https://doi.org/10.1016/J.CEP.2016.07.007.
Simakova, I.L., Demidova, Y.S., Murzina, E.V., Aho, A., Murzin, D.Y., 2016. Structure Sensitivity in Catalytic Hydrogenation of Galactose and Arabinose over Ru/C Catalysts. Catal Letters 146 (7), 1291–1299.
Smeds, A.I., Vähäsalo, L., Rahkila, J., Eklund, P.C., Willför, S.M., 2019. Chemical characterisation of polymerised extractives in bleached birch kraft pulp. Holzforschung 73 (11), 1017–1033.
Sricharoenchaikul, V., Pechyen, C., Aht-ong, D., Atong, D., 2008. Preparation and characterization of activated carbon from the pyrolysis of physic nut (*Jatropha curcas L.*) waste. Energy and Fuels 22 (1), 31–37.
Strano, M.S., Agarwal, H., Pedrick, J., Redman, D., Foley, H.C., 2003. Templated pyrolytic carbon: the effect of poly(ethylene glycol) molecular weight on the pore size distribution of poly(furfuryl alcohol)-derived carbon. Carbon N Y 41, 2501–2508. https://doi.org/10.1016/S0008-6223(03)00326-9.
Taylor, R., Nattrass, L., Alberts, G., Robson, P., Chudziak, C., Bauen, A., Libelli, I.M., Lotti, G., Prussi, M., Nistri, R., Chiaramonti, D., 2015. From the Sugar Platform to biofuels and biochemicals: Final report for the European Commission Directorate-General Energy, Final report for the European Commission Directorate-General Energy.
Tronconi, E., Groppi, G., Visconti, C.G., 2014. Structured catalysts for non-adiabatic applications. Curr Opin Chem Eng 5, 55–67.
UN, 2017. Resolution adopted by the General Assembly on 6 July 2017. Work of the Statistical Commission pertaining to the 2030 Agenda for Sustainable Development A/RES/71/3.
Wang, Z., Lu, Z., Huang, X., Xue, R., Chen, L., 1998. Chemical and crystalline structure characterizations of polyfurfuryl alcohol pyrolyzed at 600°C. Carbon N Y 36 (1-2), 51–59.
Weisz, P.B., Hicks, J.S., 1995. The behaviour of porous catalyst particles in view of internal mass and heat diffusion effects. Chem Eng Sci 50 (24), 3951–3958.
Wenmakers, P.W.A.M., van der Schaaf, J., Kuster, B.F.M., Schouten, J.C., 2010. Comparative modeling study on the performance of solid foam as a structured catalyst support in multiphase reactors. Ind Eng Chem Res 49 (11), 5353–5366.
Werpy, T., Petersen, G., 2004. Top Value Added Chemicals from Biomass: Volume I – Results of Screening for Potential Candidates from Sugars and Synthesis Gas. Office of Scientific and Technical Information (OSTI). Office of Scientific and Technical Information.
Xu, J., Liu, B., Wu, L., Hu, J., Hou, H., Yang, J., 2019. A waste-minimized biorefinery scenario for the hierarchical conversion of agricultural straw into prebiotic xylooligosaccharides, fermentable sugars and lithium-sulfur batteries. Ind Crops Prod 129, 269–280.
Zabner, J., Seiler, M.P., Launspach, J.L., Karp, P.H., Kearney, W.R., Look, D.C., Smith, J. J., Welsh, M.J., 2000. The osmolyte xylitol reduces the salt concentration of airway surface liquid and may enhance bacterial killing. Proc Natl Acad Sci U S A 97 (21), 11614–11619.
Zaharopoulou, A., Yannopoulos, S.N., Ioannides, T., 2020. Carbon Membranes Prepared from Poly (Furfuryl Alcohol–Furfural) Precursors: Effect of FeCl3 Additive. C — Journal of Carbon Research 6 (3), 53.